Title: **Human macula formation involves two waves of retinoic acid signaling suppression via *CYP26A1* regulating cell cycle exit and cone specification**

Authors/affiliations: Philippa Harding[1*], Maja Wojtynska[1], Alexander J. Smith[1], Robin R. Ali[1], Rachael A. Pearson[1*]

[1]Ocular Cell and Gene Therapy Group, Centre for Gene Therapy and Regenerative Medicine, King's College London, Tower Wing, Guy's Hospital, London, SE1 9RT, UK

[*] Co-corresponding authors - rachael.pearson@kcl.ac.uk, philippa.harding@kcl.ac.uk

6673 words

Abstract

The human macula is a specialized, M/L cone-rich region of the eye, critical for high acuity vision, but little is known about the pathways regulating its development. Transcriptional regulation by Retinoic Acid (RA) is essential for many aspects of human eye development. Here, we report a striking biphasic expression of the RA-catabolizing enzyme, *CYP26A1,* in early human macular development between post-conception weeks 6-17. Early inhibition of RA signaling in human retinal organoids (hROs) prompts early cell cycle exit, and an increase in cone photoreceptors, while late inhibition alters cone subtype specification. Conversely, *FGF8,* which is negatively regulated by RA and vital for High Acuity Area specification in chick, is not expressed in the nascent human macula and had no effect on hRO photoreceptor fate.

Keywords

Macula; fovea; Retinoic Acid; FGF8; high acuity area; cone photoreceptor; development; specification, fetal, retinal organoids

Graphical abstract:

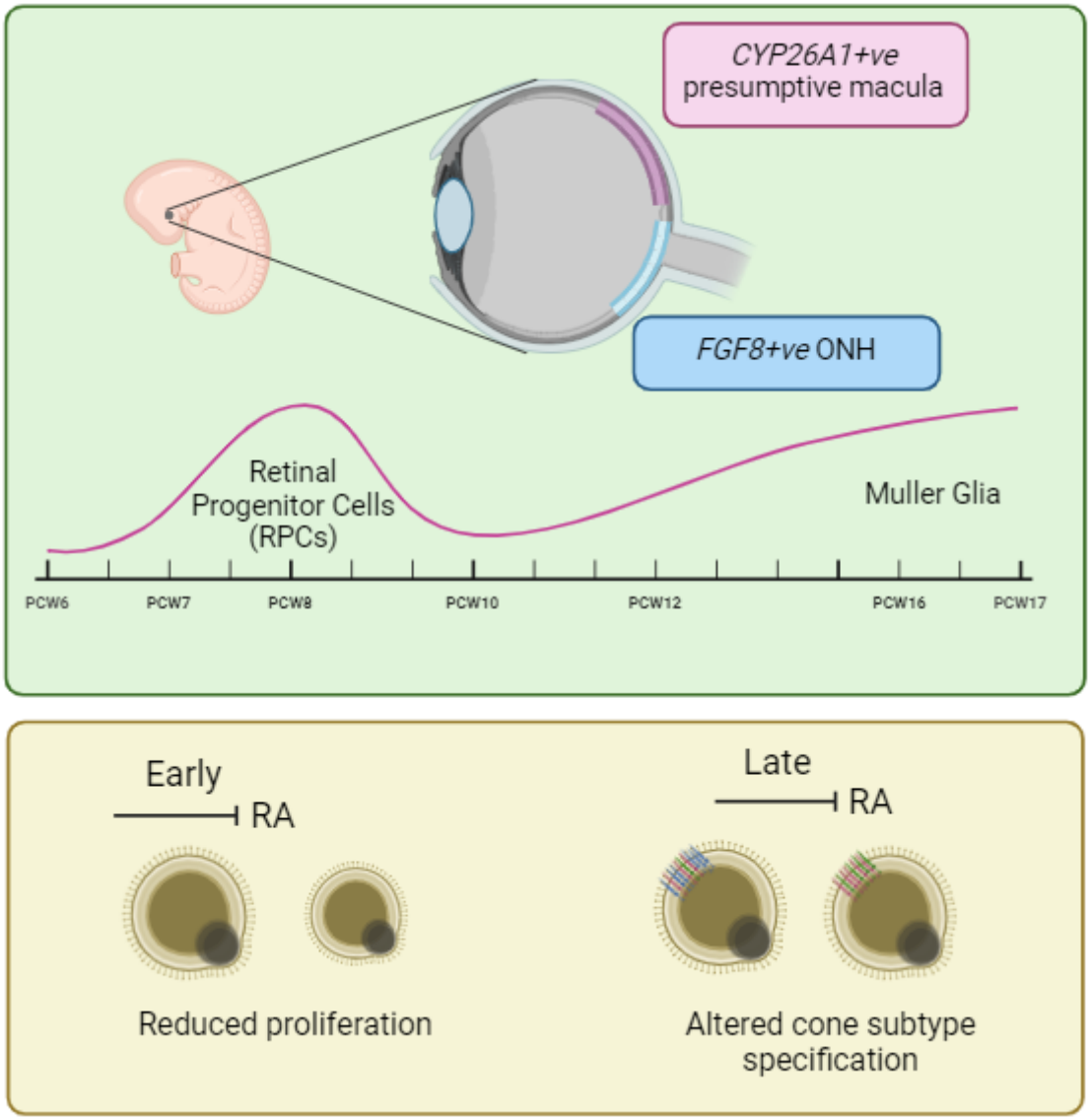

Acronyms

CMZ – Ciliary marginal zone
CS – Carnegie Stage
CYP26 - cytochrome P450 family 26
d – Day
FGF – Fibroblast growth factor
GCL – Ganglion cell layer
HAA – High acuity area
hROs – Human stem cell derived retinal organoids
INL – Inner nuclear layer
LE – Lens epithelium
mROs – Mouse stem cell derived retinal organoids
NBL – Neuroblastic Layer
ONH – Optic Nerve Head
ONL – Outer nuclear layer
PCW – Post-conception weeks
PM – Presumptive Macula
RA – Retinoic Acid
RAR – Retinoic Acid Receptor
RARE – Retinoic Acid Response Element
RFZ – Rod-free zone
RGC – Retinal ganglion cells
RPCs – Retinal Progenitor Cells
RXR – Retinoid X receptor

Introduction

The macula is a 5-6mm region at the centre of the retina critical for high acuity and color vision in humans and simian primates[1,2]. Damage and degeneration in this region lead to debilitating sight loss, significantly impacting activities such as reading, recognizing faces, and driving. The macula has a unique architecture comprising a high density of cone photoreceptors and retinal ganglion cells (RGCs), contrasting with the rod-dominant peripheral retina, as well as possessing a highly ordered synaptic configuration to aid rapid phototransduction[1,3,4]. Cone density is highest (200,000 cones/mm^2) at the very centre of the macula in the foveola, a 300µm avascular rod-free zone (RFZ) consisting exclusively of medium (M/green) and long (L/red) wavelength-detecting cones[1,3]. The proportion of cones:rods declines with increasing eccentricity, being ~1:1 in the fovea (1.85mm from the fovea centre), dropping to 1:30 in the peripheral retina[1,3].

Macular formation starts early in development, with immature cones present in the presumptive macula (PM) by post-conception week (PCW)8/Carnegie stage (CS)23[2,5]. The macula region has accelerated differentiation compared with the rest of the retina throughout prenatal development[2,6,7], but adult cone density is not achieved until 4-6 years[3,8–10]. Despite its importance, the molecular mechanisms underlying human macular development remain poorly understood, owing to the lack of equivalent structures in rodents and many other classical animal models[2,11].

In addition to humans and primates, some other species possess a broadly analogous region of the retina adapted for high acuity vision[12]. Chickens possess an RFZ, known as an *area centralis* or High Acuity Area (HAA)[12–14]. Recent research has shown that chick HAA formation is dependent on regulation of retinoic acid (RA) levels[13]. RA is a morphogen that can control gene expression through binding to retinoic acid receptors (RARs) and retinoid X receptors (RXRs), which can then engage specific DNA sequences known as retinoic acid-response elements (RAREs)[13,15]. Upon binding to RAREs, co-activators are recruited and lead to transcriptional activation of specific RA-regulated genes[15,16]. RA is synthesized by retinal dehydrogenases (ALDHA1-3) and catabolized by cytochrome P450 family 26 enzymes (CYP26s)[15,17,18]. Transcriptional regulation by RA is key to development of multiple tissues[16], including heart organogenesis[19], limb formation[20] and hindbrain patterning[21], and is essential for human eye development, as demonstrated by the range of congenital ocular conditions associated with pathogenic variants of the RA signaling pathway, including microphthalmia, anophthalmia and coloboma (MAC)[22].

Modulation of RA signaling has been implicated in the formation of HAAs in other organisms, including high expression of *Cyp26a1* by Müller glia in the zebrafish HAA at later stages of development[23]. Strong expression of *Cyp26a1/c1* was observed at a single spot at the presumptive HAA early in chick development, coincident and colocalized with *Fgf8* (fibroblast growth factor 8) expression, which is directly downregulated by RA through binding to a RARE upstream of *Fgf8* [13,16,24]. In the chick retina, RA was found to negatively regulate *Fgf8*, with transient addition of RA leading to loss of *Fgf8* expression, disruption of the RFZ, and a decrease in the high RGC density typical of the HAA. Furthermore, expression of *CYP26A1* mRNA was observed in the human PM at CS22 (PCW8). Subsequent studies have reported *CYP26A1* to be significantly upregulated in macula compared with peripheral retina through bulk and scRNAseq in mid-gestation (PCW20) and adult retina human retina[25]. *CYP26C1* was found to have no detectable expression in developing human retina in both RNAseq and *in situ* experiments[13,26]. Recently, detailed analysis of *CYP26A1* and *FGF8* expression in

Rhesus monkey found that *CYP26A1* is highly expressed in the developing macular region at day 40, after the onset of cone genesis (corresponding to human ~PCW10), while *FGF8* was not localized to the macular region[27]. However, little is known about earlier developmental stages encompassing the period of human macula specification. Evaluation of *CYP26A1* and *FGF8* expression has not been performed in human fetal retina, and a conserved functional effect of RA suppression and/or upregulated *FGF8* signaling in the initial stages of human macula specification has not been demonstrated.

Understanding macula specification is important for the utilization of human stem cell-derived retinal organoids (hROs). Stem cell-derived hROs can produce layered structures that broadly resemble the human neural retina and closely follow the timing of human retinal development[28,29]. They have wide therapeutic potential, serving as donor material for cell/graft transplantation[28,30–34], as well as preclinical models for the study of development and disease mechanisms and testing new therapeutic compounds and gene therapies. Generation of cones has been of particular interest for photoreceptor replacement therapies and attempts to improve cone density of hROs have been plentiful, such as through stage-specific inhibition of Notch signalling,[31] removal of RA[35] and manipulation of thyroid hormone signaling. To date, however, hRO protocols have failed to generate macular-like cells with *in vivo*-like spatial regionalization or the genetic signature of foveal cones[25,28,36], suggesting that more complex signaling than simple removal of RA alone is involved, while the role of FGF8 has not been examined. Here, we used *in situ* hybridisation in human fetal tissue and pharmacological manipulation in hROs to investigate the spatiotemporal expression and potential roles of RA and *FGF8* in human macular development.

Results

The RA catabolizing enzyme CYP26A1 *displays a biphasic pattern of expression in the developing human macula*

To determine expression patterns of RA catabolizing enzyme *CYP26A1* and growth factor *FGF8* in the developing human macula, RNAscope™ *in situ* hybridisation was performed on fetal retina samples between PCW6 (CS16) and PCW17 (**Figure 1**). No *CYP26A1* was visible at PCW6 (CS16/17), with weak expression first visible at PCW7 (CS18/19), localized to a single, spot-like region at the centre of the retina, approximately 1mm temporal to the optic nerve head (ONH) (**Figure 1a**), a location identified previously as the presumptive macula (PM)[6]. Within this region, *CYP26A1* was distributed throughout the neuroblastic layer (NBL), colocalizing with VSX2^{+ve} RPCs (**Figure 1b**). At the start of PCW8 (CS20-21), much stronger expression of *CYP26A1* was observed in the VSX2^{+ve} NBL (**Figure 1a)**, with expression reducing by the end of PCW8 (CS22-23), by which point some RPCs expressed the cone/bipolar progenitor marker, OTX2 (**Figure 2a**). These were distributed sparsely throughout the NBL of the entire retina, although OTX2 labelling was strongest in the PM region and, within this, in the more apically located cells (**Figure 2ai-ii**). The nascent GCL could also start to be defined in PCW8 samples (**Figure 2a**). No expression of the cone photoreceptor-specific markers RECOVERIN or RXRγ was visible at this timepoint (**Figure 2aii**). *CYP26A1* was also expressed in the lens epithelium (LE) and at low levels at the nasal edge of the retina and around the ONH at CS18-20 (**Supplementary Figure 1**). By PCW10, *CYP26A1* mRNA expression was visibly weaker in the PM region, indicating that expression is downregulated by this developmental stage (**Figure 1a, b**). Moreover, its expression was restricted to a band of VSX2+/OTX2+ cells located in the nascent INL. RXRγ+/RECOVERIN+/OTX2+ cone photoreceptors did not express *CYP26A1* and were located exclusively within a single cell layer (the nascent outer nuclear layer; ONL) at the apical edge of the presumptive macula; RXRγ+/RECOVERIN+ cones were not present in the peripheral retina at this stage (**Figure 2b**). At PCW12, *CYP26A1* expression was visibly increased, compared with PCW10, this time localizing to the basal edge of the VSX2+ INL; by PCW16/17, expression of *CYP26A1* was restricted to the VSX2+/SOX9+ developing Müller glia layer, and was not visible in the VSX2+/SOX9- presumptive bipolar cells, which express much higher levels of VSX2 than presumptive Müller glia[43,44] (**Figure 1b, Figure 2c**).

FGF8 *is not expressed in the developing macula, but instead is restricted to the Optic Nerve Head in the early human retina*

In the chick, *Fgf8* is expressed in a bullseye-like pattern overlapping with *Cyp26a1/c1* and is essential for forming the HAA[13]. In notable contrast, no *FGF8* mRNA labelling was observed in the human PM region between PCW6-10, during which macula cone precursors are born, indicating that *FGF8* is not required for cone specification in the human macula (**Figure 1**). *FGF8* was visible between PCW7-12, with expression highest during early PCW8; however, expression was restricted to around the presumptive optic stalk, similar to what has previously been reported for the macaque from 40 days gestation[27], as well as the developing mouse eye from E9.5-14.5[37] and chick eye from E2-E7[38], where it is understood to maintain Pax2 expression (**Figure 3**). Expression remained low during PCW12-17, and again was only seen at low levels and restricted to around the ONH. Overlapping co-expression of *CYP26A1* and *FGF8* was not observed at any time point examined.

Presumptive macula is located more peripheral in early development relative to its central position in the mature retina due to differential proliferation rates

In the mature adult eye, the macula is located at the centre of the retina, opposite the pupil and approximately 3.5-5.5mm temporal to the ONH[39]. At early developmental timepoints, expression of *CYP26A1* was closer to the peripheral edge of the retina than expected for the PM, relative to its more central location in the adult eye. Increased proliferation of RPCs in the peripheral, compared with central, retina has been previously demonstrated through proliferative marker staining at later timepoints in development (post-PCW8)[2]. However, due to lack of available tissue and macular markers at early stages, proliferation and how this variable growth rate affects the location of the PM has not previously been investigated. Moreover, whilst a centre-to-periphery gradient of proliferation is well known, it is less clear how this relates to the PM specifically, nor whether this region stops proliferating at a different time to the rest of the central retina.

To explore this, we examined growth and proliferation across regions of the retina throughout early development. In the first instance, we measured the distance between the centre of the region of *CYP26A1* expression and i) the peripheral edge of the retina and ii) the ONH. Distance from the centre of *CYP26A1* expression to the peripheral edge of the retina increased from 300µm at PCW7 to 9000µm at PCW17, growing in a linear manner (R^2=0.96) (**Figure 4ai-iv**). The distance from the centre of *CYP26A1* expression with respect to the ONH also grew in a linear manner (R^2=0.94), from 400µm at PCW7 to 6000µm at PCW17 (**Figure 4ai-iv**). However, comparing the rates of growth, the increase in distance between the macula and periphery was approximately two-fold higher, compared with the macula to ONH distance (a rate of 114µm/day and 62µm/day respectively, p>0.001). Notably, while the macula-to-periphery distance increases from 20% of the total retina length at PCW7 to 45% at PCW17, macula-to-ONH remains constant at 30% (**Figure 4av**). This shows that the distance between the macula and the peripheral edge of the retina increases at approximately twice the rate of the central region, and that the *CYP26A1*+ macula region is located more temporally early in development and shifts closer, relative to total retinal length, to the ONH as the peripheral retina grows.

We next examined regional proliferation using the proliferative marker KI67. Consistent with the expected centre-to-periphery gradient of maturation, between CS18 and CS23, the proportion of cells that were KI67+ was higher at all timepoints in the peripheral retina compared with the central retina, with twice as many KI67+ cells at CS23 (CS18: 47% ±13.6 vs 66% ±4.7, n=3; CS20: 36% ±3.4 vs 68% ±11.6, n=3; CS23: 22% ±3.7 vs 45% ±19.1, n=3) (**Figure 4bi-ii; Supplementary Figure 2a**). This difference was statistically significant at CS20, and close to statistical significance at CS18 and CS23, likely due to low sample sizes (CS18: $t(2)=3.3$, $p=0.08$; CS20: $t(2)=6.4$, $p=0.02$; CS23: $t(2)=2.5$, $p=0.13$) (**Figure 4bi-ii**).

In addition to comparing proliferation in the central and peripheral regions, we also explored potential differences between the PM and a region in the nasal retina equidistant from the periphery as the macula, i.e. at the equivalent region of the central-peripheral gradient. (**Figure 4biii; Supplementary Figure 2a-b**). Both the macular and nasal regions showed significant reductions in the proportion of proliferating cells between CS18 and CS20/CS23 (**Figure 4biii**). However, linear regression showed that the slope in the macula region was nearly twice as steep as that of the equivalent nasal region between CS18 and CS20 (-15.6%/day and -8.6%/day, respectively, p=0.046), indicating the rate at which

proliferation slows is twice as fast in the macula across this time window (**Figure 4biv, Supplementary Figure 2c**).

At the earliest timepoint, CS18, the macula had one of the highest proportions of KI67+ cells of any region, similar to the periphery (mean of 65% ±6.3 vs 66% ±4.7), while the central/nasal regions had lower proportions of KI67 expressing cells (mean of 47% ±13.6 vs 56% ±1.6) (**Figure 4bii-iii, Supplementary Figure 2b**). However, the number of proliferating cells in the macula halved by CS20, resulting in a similar mean to the central retina by this timepoint (33% ±5.4 vs 36% ±3.4), which persisted to CS23 (24% ±7.3 vs 22% ±3.7). Notably, this reduction in proliferation rate is coincident with the timing of *CYP26A1* expression.

Human stem cell-derived retinal organoids express components of RA synthesis pathway during early differentiation, demonstrating similarity to peripheral retina development

We next sought to examine the impact of RA signaling on hRO differentiation to better understand its role in macula formation. We have previously reported that a 2D/3D differentiation protocol yields hROs from pluripotent stem cells and that this method faithfully replicates the timing of human retinal development[28] (**Supplementary Figure 3a**). This protocol involves the addition of RA from day 70 (d70) onwards and yields retinas with ~1:4 ratio of cones:rods, a proportion similar to the outer edges of the macula[3]. We therefore explored the expression of components of RA metabolism and FGF8 signaling in hROs generated using this method in the first instance.

The RA synthesizing enzymes, *ALDH1A1* and *ALDH1A3,* were both upregulated early in differentiation, at the time of hRO picking, at ~d40, compared with undifferentiated hESCs, followed by a steady downregulation of *ALDH1A1* to d90 (**Figure 5a-b**). In contrast, qRT-PCR analysis showed limited expression of *CYP26A1* in d40 hROs, but this was subsequently upregulated at d80, following exogenous addition of RA to culture medium at d70, and by which time photoreceptor specification has already occurred (**Figure 5c, Supplementary Figure 3**). CRABP2 binds to cytoplasmic RA and traffics it to the nucleus for regulation of gene expression[40]. As *all*-trans retinoic acid concentration increases (atRA), so *CRABP2* expression is concomitantly upregulated, making it a proxy for circulating RA levels[40]. In hROs, *CRABP2* was upregulated at d40, compared with undifferentiated hESCs, and continues to increase throughout differentiation, but significantly increases beyond d70, when exogenous RA is added. This demonstrates that endogenous RA signaling occurs throughout hRO differentiation, and the pathway is, unsurprisingly, significantly upregulated following addition of exogenous RA (**Figure 5d**). RA signaling and lack of *CYP26A1* expression prior to cone specification in hROs points to a more peripheral retina-like molecular developmental program in hROs produced using this protocol.

Expression of *FGF8* mRNA was significantly increased by d40 of differentiation compared with undifferentiated hESCs, with expression levels then steadily decreasing throughout differentiation, up to d90 (**Figure 5e**). mRNA expression for FGF receptors *(FGFR)1-4* was detected in hESCs d0 (CT values 25-35); however, expression of *FGFR1/2/4* significantly decreased over the course of hRO differentiation, while *FGFR3* expression increased significantly between d0 and d40, followed by subsequent slowly decreasing expression between d40-d90 (**Figure 5f**).

253 *Early inhibition of RA by AGN193109 leads to smaller hROs and reduced proliferation*
254
255 Based on mRNA expression and immunostaining analysis showing onset of cone specification by d40
256 of differentiation (**Supplementary Figure 3**), hROs were dosed with pan-Retinoic Acid Receptor (RAR)
257 antagonist AGN193109 (10µM)[41] or recombinant growth factor FGF8 (rFGF8) (100ng/ml) initially with
258 for a single pulse (early) from d42-50 of differentiation in order to mimic the early phase of *CYP26A1*-
259 induced RA catabolism, as seen in the human PM during PCW7-8. Dosing concentrations was
260 determined using a dose-response viability assay and effect on gene expression (**Supplementary**
261 **Figure 4**). Early dosing with 10µM AGN193109 significantly reduced expression of *CRABP2* ($t(2)=5.77$,
262 $p=0.03$), demonstrating reduced levels of circulating RA[40] (**Supplementary Figure 5a**).
263
264 Given the rapid reduction in proliferative cells observed in the RPCs of the macula during the first phase
265 of *CYP26A1* expression, relative to other regions of the retina (**Figure 4a**), we first examined growth
266 rates in hROs dosed with RA inhibitor AGN193109. Measurements of hRO size before and after early
267 dosing showed RA inhibition led to a very significant reduction in growth by day 60, compared with
268 DMSO-treated control hROs ($t(32)=5.18$, $p<0.0001$) (**Figure 6a**). Quantification of immunostaining with
269 proliferative marker KI67 showed a significantly reduced percentage of KI67+ cells in AGN193109-
270 dosed hROs ($t(24)=2.48$, $p=0.02$), while no difference in apoptotic marker CASPASE-3 was observed
271 ($t(29)=0.64$, $p=0.5$), indicating that the reduction in growth in RA-inhibited hROs was due to lower
272 levels of proliferation, rather than exacerbated cell death (**Figure 6b**). These data indicate that early
273 inhibition of RA in RPCs leads to increased cell cycle exit, which may uncover the role of the first phase
274 of *CYP26A1* expression in the developing human macula at PCW7-8.
275 *Early pharmacological inhibition of RA signaling in hROs increases expression of photoreceptor*
276 *markers, while addition of recombinant FGF8 has no effect, mimicking in vivo macula formation*

277 Since application of AGN193109 led to a reduction in RPC proliferation, but no change in cell death, it
278 is plausible to assume that RPCs are being induced to exit the cell cycle prematurely. We therefore
279 examined whether this had any effect on the adoption of early born cell fates (predominantly cone
280 photoreceptors and RGCs). Transient early inhibition of the RA pathway led to significant increases in
281 the expression of the pan-photoreceptor marker *RECOVERIN* ($t(5)=2.56$, $p=0.05$), at d60, along with
282 cone progenitor maker *OTX2* ($t(4)=4.58$, $p=0.01$), while expression of the cone precursor markers, *RXRγ*
283 and *THRβ,* also slightly increased, although were not significant ($t(5)=1.45$, $p=0.2$); ($t(5)=1.69$, $p=0.15$,
284 respectively) (**Figure 6ci**). No significant changes were observed in the expression of RPC marker *VSX2*
285 ($t(5)=1.39$, $p=0.2$) (**Figure 6c**) or RGC marker *RBPMS* and RGC/bipolar/amacrine marker *ISLET1*
286 ($t(4)=1.02$, $p=0.37$; $t(4)=0.30$, $p=0.78$, respectively) (**Supplementary Figure 5b**). Quantification of
287 immunostaining showed a significant increase in the proportion of cone progenitor cell marker OTX2+
288 cells in RA-inhibited hROs ($t(28)=2.4$, $p=0.02$), reflecting gene expression analysis (**Figure 6d**). Also
289 consistent with gene expression analysis, no change in the proportion of VSX2+ RPCs ($t(29)=0.01$,
290 $p=0.99$) or cone precursor marker RXRγ was observed ($t(26)=0.96$, $p=0.35$) (**Figure 6d, Supplementary**
291 **Figure 5c**). Conversely, addition of rFGF8 between d42-50 did not lead to any changes in RPC or
292 photoreceptor marker expression compared with PBS dosed controls (*RECOVERIN*: $t(2)=0.22$, $p=0.85$;
293 *OTX2:* $t(2)=2.99$, $p=0.10$; *RXRγ*: $t(3)=0.23$, $p=0.83$; *THRβ:* $t(2)=1.01$, $p=0.40$; *VSX2*: $t(3)=0.39$, $p=0.72$)
294 (**Figure 6cii**). These results indicate that early inhibition of RA signaling leads to early exit from the cell
295 cycle and the generation of early-born OTX2+ cone progenitor cells.

Early and late RA inhibition, mimicking biphasic CYP26A1 expression, results in increase in M/L-OPSIN, indicating a role in cone subtype specification

To investigate the effect of the early and late phases of *CYP26A1* expression, hROs were dosed with an early dose of AGN193109 between d42-50, alongside a second dose at d70-80 (early+mid) or a second and third dose at d120-130 (early+mid+late). At d150, no changes in rod marker *RHODOPSIN* expression ($t(2)=1.03$, $p=0.41$; $t(3)=0.65$, $p=0.76$; $t(3)=2.43$, $p=0.15$) or pan-cone marker *ARRESTIN-3* ($t(2)=0.82$, $p=0.50$; $t(3)=0.43$, $p=0.88$; $t(3)=1.22$, $p=0.46$) were observed between any AGN193109-dosed organoids and DMSO controls (**Figure 7a**). Dosing with AGN193109 at the early timepoint alone also showed no changes in expression of blue-wavelength detecting cone marker *S-OPSIN*, or green/red-wavelength detecting cone markers *M/L-OPSIN*s at d150. However, additional pulses (early+mid and early+mid+late) of AGN193109 both resulted in a reduction of *S-OPSIN* ($t(3)=1.67$, $p=0.30$ and $t(3)=5.64$, $p=0.02$, respectively) and an increase in *M/L-OPSIN* mRNA expression at d150 approaching significance ($t(3)=1.70$, $p=0.29$; $t(3)=2.37$, $p=0.16$), indicative of the M/L-cone-rich fovea[42] (**Figure 7a**). Expression of both *M-* and *L- OPSIN* showed no change with early dosing but higher expression with both early+mid and early+mid+late dosing, although *L-OPSIN* showed a far greater fold change (*M-OPSIN* 1.5x, *L-OPSIN* 8x), and only early+mid+late *L-OPSIN* approached significance ($t(3)=2.70$, $p=0.07$). Immunostaining of early+mid+late dosed hROs found no significant difference in the proportion of RHODOPSIN/ARRESTIN expressing cells, or the proportion of M/L-OPSIN+/ARRESTIN-3+ cells, but RA inhibition led to a significant reduction in S-OPSIN+/ARRESTIN-3+ expressing cells ($t(11)=3.14$, $p=0.01$) (**Figure 7b**).

In addition, all doses (early; early+mid; early+mid+late), RA-inhibited hROs showed upregulation of the WNT inhibitor, *SFRP1,* at d150, although this was only statistically significant for early+mid+late ($t(2)=2.02$, $p=0.18$; $t(3)=2.45$, $p=0.15$; $t(3)=5.04$, $p=0.02$, respectively) (**Figure 7ci**). Early dosing also showed a significant increase in *SFRP1* expression at d60 ($t(4)=4.50$, $p=0.01$) (**Figure 7cii**).

Taken together, this indicates that suppression of RA signaling mediated by the later phase of *CYP26A1* expression is important for specifying green/red cones in the human fovea, and that the effects of both early and late RA inhibition may involve inhibition of WNT signaling through SFRP1.

327 **Discussion**
328 In this study, we provide the first detailed spatiotemporal analysis of *CYP26A1* and *FGF8* expression in
329 human fetal retina. We also investigated the roles of these pathways in macular development through
330 manipulation of hROs. Our aim was to begin to unravel the precise functional roles of these pathways
331 in producing the specialized cellular structure of the human macula.
332
333 Analysis of early-stage human macular development has been very limited to date, with small sample
334 sizes due to scarcity of samples. The earliest previous *in situ* spatial analysis of *CYP26A1* expression in
335 human fetal retina was CS22-23 (late PCW8), which showed expression in the presumptive macula
336 (PM) at CS22 but switched off at CS23[13]. Here, we have defined the developmental timeline of *CYP26A1*
337 expression, which shows a previously unreported and striking biphasic pattern of expression in the
338 PM. The first phase of expression is initiated in the PM at PCW7 (CS18), prior to cone specification, and
339 is maintained in RPCs until the end of PCW8. By PCW10, *CYP26A1* expression in the RPCs is markedly
340 reduced. Closer examination of the PM region showed that during PCW7-8, *CYP26A1* is expressed by
341 RPCs but not by cone photoreceptor precursors, which are born by PCW10 and are localized to the
342 most apical layer of the PM. The second phase of expression begins from PCW12 and is restricted to
343 Müller glia residing in the INL of the retina, but not expressed in the developing bipolar cells.
344
345 Our findings are supported by a very recent report of *CYP26A1* expression in rhesus macaque
346 development[27], which presented strong *CYP26A1* expression in the macular region. However, in the
347 macaque, *CYP26A1* expression was only assessed after cone specification (from day 40), by which time
348 RXRγ+ cone precursor marker was expressed in the NBL of the macular region; this is equivalent to
349 around PCW10 in the human retina (~25% through gestation)[5]. In both human and macaque retina,
350 *CYP26A1* was only expressed in RPCs during the early macular formation, with no *CYP26A1* mRNA
351 observed in the OTX2+/RXRγ+/RECOVERIN+ cone precursor cells of the ONL. We also observed similar
352 *CYP26A1* expression outside the PM in LE, CMZ and around the ONH in early (PCW7-8) development
353 as reported in macaque, although the level of expression relative to the PM, appears much lower in
354 the human fetal samples compared with the monkey retina[27]. Our observation of *CYP26A1* expression
355 in the Müller glial cells after PCW12 is consistent with previous descriptions for the later stages of HAA
356 maturation in the Zebrafish[23] and the mature primate macula in the macaque[27], as well as
357 transcriptomic data for foveal Müller cells in adult human retina[25]. Taken together, we propose a
358 biphasic model of *CYP26A1* expression in the macula, with the first wave onset at PCW7-8 in RPCs,
359 followed by a second phase from PCW12, specific to Müller glia.
360
361 In striking contrast to HAA formation in the chick[13], *FGF8* was not expressed in the PM at any time
362 between PCW6 and PCW17 of development nor exhibited any spatial overlap with *CYP26A1*
363 expression, indicating that it does not play a role in human macula formation or macula cone
364 differentiation. *FGF8* mRNA was instead found around the ONH during the same period of
365 development. This is also consistent with the macaque retina, where an ONH-to-periphery gradient of
366 *FGF8* expression was observed[27]. Moreover, we found addition of rFGF8 to hRO cultures had no impact
367 on photoreceptor marker expression. As such, this demonstrates a notable divergence in the molecular
368 mechanisms underlying high acuity region development in different species.
369
370 We next sought to explore the potential functions of RA inhibition in human macular development by
371 manipulating RA signaling in hROs via pharmacological inhibition of RARs[41] in hROs to mimic *CYP26A1*

372 expression. Increased proliferation of RPCs in the periphery, compared with the central retina, has
373 previously been reported for developmental timepoints after PCW8 in human tissue[2,6] and after fetal
374 d80 in marmoset[45]. However, due to lack of markers and access to tissue, regional variation in
375 proliferation, including the macula, has not been shown for earlier stages of development. We found
376 that RPCs of the macula had the highest proportion of proliferative cells at CS18, but that this reduced
377 at twice the rate of the equivalent nasal region by CS23. Indeed, the proportion of proliferative cells
378 was already significantly reduced by CS20, coincident with *CYP26A1* expression. This suggests that
379 inhibition of RA via *CYP26A1* is required to encourage cell cycle exit. Early inhibition of RA signaling in
380 hROs supports this notion, with a significant growth reduction compared with controls. Furthermore,
381 staining with KI67 showed significantly fewer proliferating cells in dosed organoids. Thus, we propose
382 that a reduction in RA signaling caused by *CYP26A1* during the first phase of expression encourages
383 cell cycle exit of RPCs within the PM. Furthermore, hROs treated early with RAR antagonist displayed
384 an increase the number of cone-biased progenitors at d60, consistent with early cell cycle exit of RPCs
385 leading to differentiation of early-born cell types, particularly cones, which dominate the macula. This
386 aligns with our previous data investigating the effects of exogenous RA on mouse ESC-derived retinal
387 organoids (mROs), which found a short pulse of RA from d14-16 (cone precursor stage) led to an
388 increase in S-phase cells and overall cell yield, indicating RA promotes cell proliferation in RPCs[31].
389
390 Cone subtypes are determined by two fate check points: first, between S or M/L fate, and if the latter,
391 between M- or L-OPSIN expression[46]. When RA signaling was inhibited early in differentiation, prior to
392 cone specification, no change in cone subtype at d150 was observed. However, RA inhibition during
393 both mid and late hRO differentiation, after cone specification, led to upregulation of *M/L-OPSIN* and
394 a significant downregulation of *S-OPSIN* gene expression. Whilst no significant change in the
395 proportion of M/L-OPSIN protein expressing cells occurred, a significant reduction in S-OPSIN
396 expressing cells was seen. This is notable since the central retina contains a higher density of medium
397 (M)/long (L) wavelength-detecting cones than short (S) wavelength cones, which dominate the
398 peripheral retina, and the human foveola at the centre of the macula exclusively contains M/L-cones[42].
399 Interestingly, a similar effect of *CYP26A1*-mediated promotion of M-cone identity has been reported
400 in *VAX2* knockout mice, where lack of *VAX2*-mediated restriction of *CYP26A1* expression to a stripe in
401 the central retina leads to the expansion of M-cones into the typically S-cone dominated ventral
402 retina[47]. Moreover, addition of exogenous RA to mROs after cone precursor specification led to
403 upregulation of S-opsin but no change in Arrestin-3 expression, indicating that alterations in RA
404 signaling later in development also regulates cone subtype specification in mouse development[28]. In
405 our hands, pulses of RA inhibition early+mid+late in hROs led to an increase *L-OPSIN* expression,
406 broadly aligning with a recent report by Johnston and colleagues indicating that sustained application
407 during the same period of differentiation (d43-d130) of RA suppresses L-cone formation, whilst
408 promoting M-cone fate[48], albeit that we did not see a downregulation of *M-OPSIN*.
409
410 Recent scRNAseq data of human fetal retina has shown that the WNT pathway inhibitor *SFRP1* is
411 expressed in early RPCs and, later in development, by Müller glia, with strongest expression in the cells
412 of the macula, confirmed by *in situ* hybridisation at PCW18[11]. Thus, *SFRP1* shows a remarkably similar
413 biphasic and spatiotemporal expression pattern to *CYP26A1* in human fetal retina. Both early and late
414 inhibition of RA signaling in hROs led to a significant upregulation of *SFRP1*, indicating that *CYP26A1*-
415 mediated RA inhibition leads to suppression of the WNT signaling pathway. Canonical WNT signaling
416 commonly regulates proliferation through binding of β-catenin; it is plausible, therefore, to speculate

that SFRP1-induced inhibition of the WNT-β-catenin pathway may induce cell cycle exit in early RPCs, which leads to lineage specification of cone precursors[49]. Wnt signaling has been shown to play a role in maintaining RPCs in a proliferative state in Drosophila[50], zebrafish[51], *Xenopus*[52] and mice[53]. Notably, however, in chick, Wnt was not found to alter progenitor proliferation, but instead promotes expression of markers associated with peripheral retinal cell fate, ciliary body and iris[54]. This divergence in Wnt pathway function between human and chick may help explain the lack of *FGF8* expression in the presumptive human macula, in contrast to the previously established co-expression with *Cyp26a1/c1* in the chick HAA[13].

Together, these data show for the first time a biphasic pattern of expression of *CYP26A1* across human macula development. Conversely, *FGF8* expression is restricted to the region around the ONH and does not exhibit any spatial overlap with *CYP26A1*, in contrast to the chick suggesting an important divergence of regulatory mechanisms in high acuity specification. We propose novel roles for the two phases of RA inhibition in macular formation: the early wave of RA inhibition (PCW7-8) stimulates RPCs to exit the cell cycle, encouraging cone generation, while the second, later phase (from PCW12) plays a role in specification of cone subtypes. Upregulation of *SFRP1* following RA inhibition in hROs indicates that either, or both, of these processes may involve *SFRP1*-mediated WNT inhibition, although further work is required to test this directly.

This work bridges a gap in fundamental knowledge of the molecular mechanisms underlying human macular development and highlights the importance of studying human development in both animal models and human-derived tissue. These results open two avenues of future developmental research: 1) can we resolve the molecular network downstream of *CYP26A1* to establish how these pathways generate the unique structure of the human macula; and 2) what are the drivers of *CYP26A1* expression in the human PM and how are they initiated? Elucidating these molecular mechanisms could provide strategies to encourage formation of more macular-like cellular structure in *in vitro* models, which may be used to study macular development and disease, provide a preclinical model for drug testing to treat macular degeneration and improve efficacy of cells used for transplantation therapies which could restore visual function in patients by cell transplants.

446 **STAR Methods**

447 Resource Availability

448 Corresponding Author - Further information and requests for resources and reagents should be
449 directed to and will be fulfilled by the corresponding author, Rachael Pearson
450 (rachael.pearson@kcl.ac.uk).

451

452 Materials Availability

453 This study did not generate new unique reagents.

454

455 Data and Code Availability

456 Mean data is presented as mean ±SD, as indicated in figure legends. This paper did not generate
457 original code. Any additional information/data is available from the corresponding contact upon
458 request.

459

460 Human fetal retina sample collection

461 Human fetal retina samples were collected from the Human Developmental Biology Resource
462 (http://www.hdbr.org/) with research ethics approval and informed consent (Project Number 200599).
463 Samples were stored in full compliance with the Human Tissue Act 2004.

464

465 Differentiation of retinal organoids

466 Human PSCs were maintained on Geltrex-coated six-well plates in E8. Human retinal organoids (hROs)
467 were generated from the H9 ESC line according to a previously published protocol[28]. In brief, hESCs
468 were maintained to 90% confluency, then on day 1 (d1) E6 medium was added for 2 days, followed by
469 Proneural Induction Medium (PIM), which was changed every 2-3 days. Cultures were maintained in
470 PIM for up to 40 days, during which time hROs started to appear and were individually excised and
471 transferred to low-binding 96-well plates, where they were maintained in 3D culture in Retinal
472 Differentiation Media (RDM). At d42, additional factors were added to the RDM (RDM+F) which were
473 maintained until d70. On d70, individual hROs were transferred into low-binding 24-well plates and
474 Retinoic Acid (RA) was added fresh to the RDM+F at a concentration of 1mg/ml. On d90, hROs were
475 transitions to Retinal Differentiation Medium (RDM90), to which fresh RA was added at a
476 concentration of 0.5mg/ml[28].

477

478 Fetal retina/hRO sample preparation for immunohistochemistry/RNAscope™

479 For immunohistochemistry (IHC)/RNAscope™, human fetal samples were fixed for 1 day in 10%
480 formalin before transferring to PBS. Samples were incubated overnight in 20% (w/v) sucrose, prior to
481 cryo-embedding in OCT matrix. Tissue was cut at 10µM thickness. hROs were washed with PBS and
482 fixed for 1 hour in 4% PFA, followed by PBS wash and incubated overnight in 20% (w/v) sucrose, prior
483 to cryo-embedding in OCT matrix. Tissue was cut at 10µM thickness, mounted on Superfrost glass
484 slides, air-dried overnight and frozen at -20°C.

485 RNAscope™ *in situ* hybridisation
486 RNAscope™ Multiplex Fluorescence Assay was performed using manufacturer's protocol for fixed
487 frozen tissue with manual antigen retrieval. In short, samples were baked at 60°C for 30 minutes,
488 postfixed with 4% PFA for 15 minutes at 4°C then dehydrated using an ethanol gradient, before 10-
489 minute treatment with hydrogen peroxidase. Manual antigen retrieval was performed at 80°C for 5
490 minutes, then sections were pretreated with protease III for 30 minutes at 40°C. Sections were
491 incubated with probe Hs-CYP26A1-C1 (#487741) and Hs-FGF8-C2 (#415791-C2) for 3 hours at 40°C,
492 before storing in 5xSSC overnight. Probes went through series of amplification steps, before developing
493 the signal and labelling each with OPAL cyanine 3/5 fluorophores, respectively. Slides were then
494 counterstained with VSX2 and Alexa-fluor 488 and DAPI according to the IHC protocol below and
495 mounted in DAKO mounting medium. For **Figure 1**, sample numbers were as follows: CS16/17: n=3,
496 CS18/19: n=2, CS20/21: n=4, CS22/23: n=4, PCW10: n=3, PCW12: n=2, PCW16/17: n=2. Regional length
497 measurements were taken using ImageJ and fitted and analyzed using linear regression analysis in
498 GraphPad Prism (v10.1.2).
499
500 Immunohistochemistry (IHC)
501 Cryosections were permeabilized for 1 hour at room temperature with PBS/0.1% Tween/0.5% Triton
502 X, then blocked for 2 hours at room temperature with PBS/0.1% Tween/5% donkey serum/1% BSA.
503 Primary antibodies with incubated overnight at 4°C. Alexa Fluor® secondary antibodies were incubated
504 for 1 hour at room temperature at 1:400 dilution, along with DAPI counterstain. Confocal images were
505 taken using a Leica DM5500Q and processed in ImageJ. Spot count analysis was performed using Imaris
506 10.0. For analysis of KI67 in human fetal tissue, the same length of region was selected at different
507 regions of the same retina: the macula (identified by *CYP26A1*+ staining); the central region between
508 the macula and nerve; the region the same distance as the macula from the periphery on the nasal
509 side of the retina; and the periphery (Supplementary Figure 2a). For analysis of CAPSASE staining in
510 hROs, necrotic core was masked to ensure only cell death in the neural retina cells was included
511 (**Supplementary Figure 6**). Antibodies are listed in **Supplementary Table 1**. Analysis was performed
512 using unpaired t-tests.
513
514 qPCR gene expression analysis
515 For all qPCR assays, 3-5 hROs were pooled for each sample depending on collection timepoint (5 for
516 d40-d90, 3 for d120-150). Samples were taken from independent experiments and a minimum of n=3
517 independent samples were used for analysis. RNA was extracted from hRO pellets using RNeasy Micro
518 kit (Qiagen), according to manufacturer's instructions. Samples were eluted in 30µl and stored at -
519 80°C. Concentration and RNA quality analyzed using a BioDrop. cDNA was synthesized using
520 QuantiTect Reverse Transcription Kit, according to manufacturer's instructions. Quantitative RT-PCR
521 was performed using Perfecta Low-ROX MasterMix with custom primers listed in **Supplementary Table**
522 **2** and probes from the Merck Universal Probe library or PowerTrack SYBR MasterMix with ROX as
523 passive reference. All samples were run in triplicate alongside 2 endogenous reference genes (*GAPDH*
524 and *β–actin*), along with water and no RT negative controls. Comparative CT was calculated to
525 determine relative gene expression as fold change from either d0 PSCs or undosed controls[55].

526 AlamarBlue viability assay

527 Optimal dosing concentrations of recombinant FGF8 and AGN193109 were determined using cell
528 viability analysis by Alamar blue (**Supplementary Figure 4**). AlamarBlue utilizes resazurin which is
529 reduced in presence of living cells and is non-toxic/cell permeable. Organoids were kept in separate
530 wells of a 96-well plate and incubated for 4 hours with 10% AlamarBlue diluted in media, after which
531 AlamarBlue was transferred to a new 96 well plate, organoids were washed 3 times with PBS and
532 returned to media. Fluorescence of AlamarBlue at 590nm (RFU) was then measured using a plate
533 scanner and % reduction calculated using:

534

535

536 $$Reduction_{AB} = \frac{RFU^{Exp} - RFU^{Neg}}{RFU^{100\%} - RFU^{Neg}} \times 100$$

537

538 In which $Reduction_{AB}$ is the percentage reduction of AlamarBlue, RFU^{Exp} is the Relative Fluorescence
539 Units (RFU) for the experimental sample, RFU^{Neg} is the RFU for the Negative control, and $RFU^{100\%}$ is
540 the RFU for the 100% reduced positive control.

541

542 To control for differences in hRO size, change in reduction from day 0 was calculated for each hRO:

543

544 $$\Delta Reduction = Reduction_{AB}^{Day\ X} - Reduction_{AB}^{Day\ 0}$$

545

546 Relative change in viability of treated organoids was normalized to DMSO treated controls:

547

548 $$\Delta Viability = \frac{\Delta Reduction^{Exp}}{\Delta Reduction^{Control}} \times 100$$

549

550 In which *ΔViability* is the change in viability from Day 0 in the experimental sample relative to the DMSO-
551 dosed control sample

552

553 As hRO viability was not significantly reduced upon dosing with 10µM AGN19309, but was significantly
554 reduced upon dosing with 20µM AGN19309, 10µM AGN19309 was used for all following experiments.
555 No reduction in viability was observed at any concentration of rFGF8.

556

557 FGF8 can self-regulate its mRNA expression[56]. Consequently, expression of *FGF8* was assessed
558 following dosing with rFGF8. No significant difference in *FGF8* expression was observed at any
559 concentration, however, the largest mean difference was found at 100ng/µl. Consequently, this
560 concentration was used for all following experiments.

561 hRO growth analysis

562 Growth of hROs was analyzed by measuring organoid area with ImageJ from brightfield images taken
563 at d42 (prior to dosing) and d54 (4 days post-dosing), from which % increase in area size calculated.
564
565 Statistics
566 All means are presented as mean ±SD; N denotes number of independent experiments (i.e.,
567 differentiation batches) and n denotes number of images or hROs examined, where appropriate.
568 Statistical testing was performed in GraphPad Prism (version 10.1.2). Tests used to analyze statistical
569 significance (normality testing, paired t-tests, one-way ANOVAs) are specified in figure legends.

Acknowledgements

This research was funded by Fight for Sight (5139/5140), and Medical Research Council UK (MR/T002735/2). Maja Wojtynska was funded by the Wellcome Trust as part of the Advanced Therapies for Regenerative Medicine Wellcome Trust PhD Program (218461/Z/19/Z). This work was made possible by the support, dedication and teamwork of the Ocular Cell and Gene Therapy, with particular thanks to Dr E West, Dr M. Branch, Dr M. Khazim, B. Ladino, J. Kapadia, E. Lanning, M. Margari, M. Tariq, C. Mofidi, K. Kumar, S. Guilfoyle, S. van Heerden for help with stem cell maintenance cultures. For the purpose of open access, the authors have applied a Creative Commons Attribution (CC BY) licence to any Author Accepted Manuscript version arising.

Author Contributions

Conceptualization – PH, RP; Data curation – PH, MW; Formal Analysis – PH; Funding acquisition – RP; Investigation – PH, RP; Methodology – PH; Supervision – RP; Visualization – PH; Writing – original draft – PH; Writing – review & editing – PH, AS, RA, RP

Declaration of Interests

The authors declare no competing interests.

587 **References**

588 1. Voigt, A. P. *et al.* Human photoreceptor cells from different macular subregions have distinct
589 transcriptional profiles. *Hum. Mol. Genet.* **30**, 1543–1558 (2021).
590 2. Hoshino, A. *et al.* Molecular Anatomy of the Developing Human Retina. *Dev. Cell* **43**, 763-
591 779.e4 (2017).
592 3. Curcio, C. A., Sloan, K. R., Kalina, R. E. & Hendrickson, A. E. Human photoreceptor topography.
593 *J. Comp. Neurol.* **292**, 497–523 (1990).
594 4. Provis, J. M. & Hendrickson, A. E. The Foveal Avascular Region of Developing Human Retina.
595 *Arch. Ophthalmol.* **126**, 507–511 (2008).
596 5. Hendrickson, A. & Zhang, C. Development of cone photoreceptors and their synapses in the
597 human and monkey fovea. *J. Comp. Neurol.* **527**, 38–51 (2019).
598 6. Hendrickson, A. Development of Retinal Layers in Prenatal Human Retina. *Am. J. Ophthalmol.*
599 **161**, 29-35.e1 (2016).
600 7. Hendrickson, A., Possin, D., Vajzovic, L. & Toth, C. A. Histologic Development of the Human
601 Fovea From Midgestation to Maturity. *Am. J. Ophthalmol.* **154**, 767-778.e2 (2012).
602 8. Diaz-Araya, C. & Provis, J. M. Evidence of photoreceptor migration during early foveal
603 development: a quantitative analysis of human fetal retinae. *Vis. Neurosci.* **8**, 505–514 (1992).
604 9. Springer, A. D., Troilo, D., Possin, D. & Hendrickson, A. E. Foveal cone density shows a rapid
605 postnatal maturation in the marmoset monkey. *Vis. Neurosci.* **28**, 473 (2011).
606 10. Yuodelis, C. & Hendrickson, A. A qualitative and quantitative analysis of the human fovea
607 during development. *Vision Res.* **26**, 847–855 (1986).
608 11. Lu, Y. *et al.* Single-Cell Analysis of Human Retina Identifies Evolutionarily Conserved and
609 Species-Specific Mechanisms Controlling Development. *Dev. Cell* **53**, 473–491 (2020).
610 12. Mey, J. & Thanos, S. Development of the visual system of the chick: I. Cell differentiation and
611 histogenesis. *Brain Res. Rev.* **32**, 343–379 (2000).
612 13. Silva, S. da & Cepko, C. L. Fgf8 Expression and Degradation of Retinoic Acid Are Required for
613 Patterning a High-Acuity Area in the Retina. *Dev. Cell* **42**, 68–81 (2017).
614 14. Meyer, D. & May Jr, H. C. The Topographical Distribution of Rods and Cones in the Adult
615 Chicken Retina. *Exp. Eye Res.* **17**, 347–355 (1973).
616 15. Cvekl, A. & Wang, W.-L. L. Retinoic acid signaling in mammalian eye development. *Exp. Eye*
617 *Res.* **89**, 280–291 (2009).
618 16. Cunningham, T. J. & Duester, G. Mechanisms of retinoic acid signalling and its roles in organ
619 and limb development. *Nat. Rev. Mol. Cell Biol.* **16**, 110–123 (2015).
620 17. Sakai, Y., Luo, T., McCaffery, P., Hamada, H. & Dräger, U. C. CYP26A1 and CYP26C1 cooperate
621 in degrading retinoic acid within the equatorial retina during later eye development. *Dev.*
622 *Biol.* **276**, 143–157 (2004).
623 18. Thatcher, J. E. & Isoherranen, N. The role of CYP26 enzymes in retinoic acid clearance. *Expert*
624 *Opin. Drug Metab. Toxicol.* **5**, 875 (2009).
625 19. Nakajima, Y. Retinoic acid signaling in heart development. *Genesis* **57**, e23300 (2019).
626 20. Stratford, T., Horton, C. & Maden, M. Retinoic acid is required for the initiation of outgrowth
627 in the chick limb bud. *Curr. Biol.* **6**, 1124–1133 (1996).
628 21. Hernandez, R. E., Putzke, A. P., Myers, J. P., Margaretha, L. & Moens, C. B. Cyp26 enzymes
629 generate the retinoic acid response pattern necessary for hindbrain development.
630 *Development* **134**, 177–187 (2007).
631 22. Thompson, B. *et al.* Genetics and functions of the retinoic acid pathway, with special
632 emphasis on the eye. *Hum. Genomics* **13**, 1–15 (2019).
633 23. Lahne, M., Yoshimatsu, T. & MacDonald, R. B. Retinoic acid signaling in the developing
634 zebrafish high acuity zone. *Invest. Ophthalmol. Vis. Sci.* **64**, 3630–3630 (2023).
635 24. Kumar, S. & Duester, G. Retinoic acid controls body axis extension by directly repressing Fgf8
636 transcription. *Development* **141**, 2972–2977 (2014).
637 25. Cowan, C. S. *et al.* Cell Types of the Human Retina and Its Organoids at Single-Cell Resolution.

638 *Cell* **182**, 1623-1640.e34 (2020).
639 26. Chen, R. Single Cell Multiome Atlas of the Human Developing Retina. *Res. Sq.* (2023).
640 27. Krueger, M. R., Fishman-Williams, E., Simó, S., Tarantal, A. F. & La Torre, A. Expression
641 patterns of CYP26A1, FGF8, CDKN1A, and NPVF in the developing rhesus monkey retina.
642 *Differentiation* **135**, 100743 (2024).
643 28. Gonzalez-Cordero, A. *et al.* Recapitulation of Human Retinal Development from Human
644 Pluripotent Stem Cells Generates Transplantable Populations of Cone Photoreceptors. *Stem*
645 *Cell Reports* **9**, 820–837 (2017).
646 29. Li, L. *et al.* Electrophysiological characterization of photoreceptor-like cells in human inducible
647 pluripotent stem cell-derived retinal organoids during in vitro maturation. *Stem Cells* **39**, 959–
648 974 (2021).
649 30. Pearson, R. A. *et al.* Restoration of vision after transplantation of photoreceptors. *Nature* **485**,
650 99–103 (2012).
651 31. Kruczek, K. *et al.* Differentiation and Transplantation of Embryonic Stem Cell-Derived Cone
652 Photoreceptors into a Mouse Model of End-Stage Retinal Degeneration. *Stem Cell Reports* **8**,
653 1659–1674 (2017).
654 32. Gonzalez-Cordero, A. *et al.* Photoreceptor precursors derived from three-dimensional
655 embryonic stem cell cultures integrate and mature within adult degenerate retina. *Nat.*
656 *Biotechnol.* **31**, 741–747 (2013).
657 33. Ribeiro, J. *et al.* Restoration of visual function in advanced disease after transplantation of
658 purified human pluripotent stem cell-derived cone photoreceptors. *Cell Rep.* **35**, 109022
659 (2021).
660 34. Shirai, H. *et al.* Transplantation of human embryonic stem cell-derived retinal tissue in two
661 primate models of retinal degeneration. *Proc. Natl. Acad. Sci.* **113**, E81–E90 (2016).
662 35. Kim, S. *et al.* Generation, transcriptome profiling, and functional validation of cone-rich
663 human retinal organoids. *Proc. Natl. Acad. Sci.* **116**, 10824–10833 (2019).
664 36. Capowski, E. E. *et al.* Reproducibility and staging of 3D human retinal organoids across
665 multiple pluripotent stem cell lines. *Development* **146**, dev171686 (2019).
666 37. Crossley, P. H. & Martin, G. R. The mouse Fgf8 gene encodes a family of polypeptides and is
667 expressed in regions that direct outgrowth and patterning in the developing embryo.
668 *Development* **121**, 439–451 (1995).
669 38. Soukkarieh, C., Agius, E., Soula, C. & Cochard, P. Pax2 regulates neuronal–glial cell fate choice
670 in the embryonic optic nerve. *Dev. Biol.* **303**, 800–813 (2007).
671 39. Bringmann, A. *et al.* The primate fovea: Structure, function and development. *Progress in*
672 *Retinal and Eye Research* vol. 66 49–84 (2018).
673 40. Napoli, J. L. Functions of Intracellular Retinoid Binding-Proteins. *Subcell. Biochem.* **81**, 21
674 (2016).
675 41. Schubert, M. & Germain, P. Retinoic Acid and Retinoid X Receptors. *Cells* **12**, 864 (2023).
676 42. Bumsted, K. & Hendrickson, A. Distribution and Development of Short-Wavelength Cones
677 Differ Between Macaca Monkey and Human Fovea. *J. Comp. Neurol.* **516**, 502–516 (1999).
678 43. Luo, Z. *et al.* Islet1 and Brn3 Expression Pattern Study in Human Retina and hiPSC-Derived
679 Retinal Organoid. *Stem Cells Int.* **2019**, 1–14 (2019).
680 44. Wohlschlegel, J. *et al.* ASCL1 induces neurogenesis in human Müller glia. *Stem Cell Reports*
681 **18**, 2400–2417 (2023).
682 45. Hendrickson, A., Possin, D., Kwan, W. C., Huang, J. & Bourne, J. A. The temporal profile of
683 retinal cell genesis in the marmoset monkey. *J. Comp. Neurol.* **524**, 1193–1207 (2016).
684 46. Hussey, K. A., Hadyniak, S. E. & Johnston, R. J. Patterning and Development of Photoreceptors
685 in the Human Retina. *Front. Cell Dev. Biol.* **10**, (2022).
686 47. Alfano, G. *et al.* Vax2 regulates retinoic acid distribution and cone opsin expression in the
687 vertebrate eye. *Development* **138**, 261–271 (2011).
688 48. Hadyniak, S. E. *et al.* Retinoic acid signaling regulates spatiotemporal specification of human

689 green and red cones. *PLoS Biol.* **22**, e3002464 (2024).
690 49. Liu, J. *et al.* Wnt/β-catenin signalling: function, biological mechanisms, and therapeutic
691 opportunities. *Signal Transduct. Target. Ther. 2021 71* **7**, 1–23 (2022).
692 50. Kubo, F., Takeichi, M. & Nakagawa, S. Wnt2b controls retinal cell differentiation at the ciliary
693 marginal zone. *Development* **130**, 587–598 (2003).
694 51. Meyers, J. R. *et al.* β-catenin/Wnt signaling controls progenitor fate in the developing and
695 regenerating zebrafish retina. *Neural Dev.* **7**, (2012).
696 52. Denayer, T. *et al.* Canonical Wnt Signaling Controls Proliferation of Retinal Stem/Progenitor
697 Cells in Postembryonic Xenopus Eyes. *Stem Cells* **26**, 2063–2074 (2008).
698 53. Liu, H., Mohamed, O., Dufort, D. & Wallace, V. A. Characterization of Wnt signaling
699 components and activation of the Wnt canonical pathway in the murine retina. *Dev. Dyn.*
700 **227**, 323–334 (2003).
701 54. Cho, S.-H. H. & Cepko, C. L. Wnt2b/beta-catenin-mediated canonical Wnt signaling
702 determines the peripheral fates of the chick eye. *Development* **133**, 3167–3177 (2006).
703 55. Schmittgen, T. D. & Livak, K. J. Analyzing real-time PCR data by the comparative CT method.
704 *Nat. Protoc.* **3**, 1101–1108 (2008).
705 56. Crossley, P. H., Martinez, S., Ohkubo, Y. & Rubenstein, J. L. R. Coordinate expression of Fgf8,
706 Otx2, Bmp4, and Shh in the rostral prosencephalon during development of the telencephalic
707 and optic vesicles. *Neuroscience* **108**, 183–206 (2001).
708

Figures

Figure 1. *CYP26A1* shows biphasic expression localized to the macula of PCW6-17 developing human fetal retina, peaking at early PCW8 and PCW16/17.
Human fetal retina samples from PCW6-17 stained *in situ* using RNAscope™ for fibroblast growth factor 8 (*FGF8, cyan*) and RA catabolizing enzyme *CYP26A1* (*magenta*), showing *CYP26A1*+ spot-like presumptive macular (PM) region colocalizing with RPC (retinal progenitor cell) marker, VSX2 (*green*) in the neuroblastic layer between CS18-23, and basal to the VSX2+ layer at PCW12-17. (a) Whole retinal section (20x), (b) High magnification of *CYP26A1*+ PM regions (40x). White arrows indicate PM region. Sections were counterstained with nuclear marker, DAPI (*greyscale*). PCW – Post-conception Weeks. Images are representative of n≥2 samples. Scale bars - 500μm.

Figure 2. Cone progenitor markers are expressed in late PCW8 presumptive macula (PM), localized to the apical layer by PCW10 but do not co-express *CYP26A1*, while macular Müller Glia cells express *CYP26A1* in PCW17 human fetal retina. (a), At late PCW8 (CS23), OTX2 (*yellow*) is expressed in cone/bipolar-biased RPCs in the neuroblastic layer (NBL) throughout the retina, but at highest density in the PM, while no RECOVERIN (*red*) or RXRγ+ (*blue*) cone precursor markers are visible. (b), At PCW10, the PM region expresses a thick layer of OTX2+ cells in the NBL, as well as RXRγ+/RECOVERIN+ cone precursors localized to a single cell layer at the apical region of the central retina, not present in the peripheral retina. *CYP26A1* expression is restricted to the neuroblastic layer, not expressed in the RECOVERIN+/ RXRγ+/OTX2+ cone precursors. (c) At PCW17, *CYP26A1* (*magenta*) localizes to the VSX2+ (*green*)/SOX9+ (*yellow*) developing Müller glia layer, basal to the VSX2+/SOX9- developing bipolar cell layer. Müller glia cytoskeletal marker Vimentin (*VIM, red*) is clearly expressed, while no *FGF8* (*cyan*) is visible in the PM. Note stains for OTX/RECOVERIN/RXRγ and VSX2/*CYP26A1* were each performed on consecutive sections from the same respective retina for (a) and (b), and for SOX9/VIM and *CYP26A1/FGF8* in (c). Sections were counterstained with nuclear marker, DAPI (*greyscale*). PCW – Post-conception Weeks; ONL – Outer Nuclear Layer; INL – Inner Nuclear Layer; GCL – Ganglion Cell Layer. Images taken at 20x (ai/bi)/40x (aii-iii/bii-iii/c) magnification. Images are representative of n≥2 samples. Scale bars – 500μm for whole retina, 200μm for (a-b) ROIs, 100μm for (c) ROIs.

Figure 3. *CYP26A1* is highly expressed in the presumptive macula (PM) of early PCW8 (CS20) human fetal retina, while *FGF8* is localized exclusively to the optic nerve head (ONH). Representative images of CS20 fetal retina stained *in situ* for *CYP26A1* (*magenta*) and *FGF8 (cyan)*, showing strong expression of *CYP26A1* in the PM colocalizing with RPC marker VSX2 (*green*), but no *FGF8*, which is only visible in RPCs around the ONH. Assay negative control (*DapB, cyan*) and positive control (Cy5 *PPIB*, Cy3 *POLR2A, magenta*) also shown. Sections were counterstained with nuclear marker, DAPI (*greyscale*). PCW – Post-conception Weeks; ONL – Outer Nuclear Layer; INL – Inner Nuclear Layer; GCL – Ganglion Cell Layer. Images taken at 40x magnification Images are representative of n=3 CS20/21 samples. Scale bars, 100μm.

Figure 4. Higher proliferation in the peripheral retina compared with the central region results in a temporally shifted *CYP26A1*+ presumptive macula (PM) at early developmental stages (PCW7-10).
(a), (i-iii) The distance of the *CYP26A1*+ (*magenta*) PM (white arrow) to the peripheral edge of the retina (IV) increases at a significantly higher rate (over 2-fold) between PCW7-17 compared with the central region between the PM and the optic nerve head linear regression slope=114 and 62 respectively, $p<0.001$. (v), The distance between the macula to periphery as a proportion of the whole retina increases over PCW7-17 (from 20%-45%), while the distance between the macula and optic nerve remains almost constant as a proportion of the whole retina (30%), due to the slower growth of the central compared with peripheral region (linear regression slope=0.0033/-0.0004 respectively). n=14, linear regression with 95% confidence internals plotted. (b), (i) Representative images of proliferative marker KI67 (*yellow*) staining in CS18-23 human fetal retinas shows: (ii) the proportion of cells expressing KI67 was at nearly two-fold higher in the peripheral retina compared with the central region during CS18-23 at all timepoints (CS18: $t(2)=3.3$, $p=0.08$; CS20: $t(2)=6.4$, $p=0.02$; CS23: $t(2)=2.5$, $p=0.13$). (iii) The proportion of proliferating cells decreases significantly in both the macula and the equivalent

759 nasal region on the centre to peripheral gradient by CS20 (macula: $t(4)=6.50$, $p=0.003$; nasal: $t(4)=5.03$, $p=0.007$).
760 (iv) Linear regression shows that the decline in KI67+ cells in the macular region is significantly steeper than the
761 nasal region between CS18 and CS20, during which time *CYP26A1* expression is upregulated in the macula
762 (macula: -15.6, nasal: -8.7, $p=0.046$). Significance values determined by paired/unpaired t-tests: *p value<0.05,
763 **p value<0.01. n=3 samples/timepoint, data are represented as mean ±SD. Sections were counterstained with
764 nuclear marker, DAPI (*greyscale*). PCW – Post-conception Weeks. Images taken at 20x magnification. Scale bars
765 – 500μm.
766
767 **Figure 5. Differentiating human retinal organoids express retinoic acid and FGF8 pathway components**. (a)
768 Relative expression of RA synthesizing enzymes *ALDH1A1* and *ALDH1A3* mRNA across differentiation of hROs. (b)
769 immunostaining of ALDH1A1 and ALDH1A3 in d40 hROs showing expression throughout the organoid, co-stained
770 with neural retinal progenitor cell marker VSX2 (images are representative of n=3 hROs), counterstained with
771 DAPI (*greyscale*); (c-f) relative expression of (c) retinoic acid catabolizing enzyme *CYP26A1*, (d) *CRABP2,* a proxy
772 for circulating RA levels, (e) fibroblast growth factor 8 (*FGF8*) and (f) FGF receptors (*FGFR1*/2/*3*/*4*) mRNA. All data
773 shown as Log_2 fold change of CT values relative to d0 hESCs (5 pooled hROs per sample, n=3). Data normalized
774 to both *GAPDH* and *β-actin* housekeeping genes. Significance values determined by one-way repeated measures
775 ANOVA followed by Dunnett's test against control group, adjusting for multiple comparisons: *p value<0.05, **p
776 value<0.01, ***p value<0.001, data are represented as mean ±SD. Scale bars - 100μm.
777
778 **Figure 6. Dosing early hROs with RA receptor inhibitor AGN193109 results in reduced growth due to reduced**
779 **proliferation and increased cone precursor marker OTX2 expression.** (a), hRO area was measured at d42,
780 prior to dosing, and no significant difference in size was found ($t(33)=1.64$, $p=0.11$). However, following
781 dosing between d42-50, organoid size was measured at d54, and the % change in area was found to
782 be significantly lower in AGN193109 dosed hROs compared with DMSO dosed controls, demonstrating
783 reduced growth in RA inhibited hROs ($t(32)=5.18$, $p<0.0001$). (b), Immunostaining for (i) apoptotic
784 marker CASPASE-3 (*yellow*) at d60 showed no significant increase in cell death between AGN193109
785 dosed and control hRO ($t(29)=0.64$, $p=0.5$), (ii) while staining for proliferative marker KI67 (*green*)
786 showed a significant reduction in cell proliferation in RA inhibited hROs ($t(24)=2.48$, $p=0.02$). (c) (i)
787 Dosing with AGN193109 led to significant increases in photoreceptor marker *RECOVERIN* (t(5)=2.56,
788 p<0.05), and cone progenitor marker *OTX2* (t(4)=4.58, p=0.01), while early cone precursor markers
789 *RXRγ* and *THRb* show trended towards increased expression ($t(5)=1.45$, $p=0.2$)/($t(5)=1.69$, $p=0.15$), and
790 no increase in retinal progenitor cell (RPC) marker *VSX2* was observed ($t(5)=1.39$, $p=0.2$). (ii) However,
791 dosing with rFGF8 had no effect on any marker expression tested (*RECOVERIN*: $t(2)=0.22$, $p=0.85$;
792 *OTX2*: $t(2)=2.99$, $p=0.10$; *RXRγ*: $t(3)=0.23$, $p=0.83$; *THRb*: $t(2)=1.01$, $p=0.40$; *VSX2*: $t(3)=0.39$, $p=0.72$).
793 (d) Immunostaining of dosed and DMSO dosed control hROs at d60 showing a significant increase in
794 proportion of cone progenitor marker OTX2+ (blue) cells in AGN193109 dosed hROs ($t(28)=2.4$,
795 $p=0.02$). All qRT-PCR data shown as Log2 fold change of CT values relative to the mean of the DMSO
796 treated controls (5 pooled hROs per sample, n≥3, lines indicate paired samples of DMSO/AGN-dosed
797 samples from the same batch of differentiation to control for batch-batch variation.). All qRT-PCR data
798 normalized to both *GAPDH* and *b-actin* housekeeping genes. Significance values determined by
799 paired/unpaired t-tests: *p value<0.05, n ≥13, data are represented as mean ±SD. Images
800 representative of n≥13 hROs, counterstained with DAPI (*greyscale*). Scale bars - 200um.
801
802 **Figure 7. Dosing late hROs with RA receptor inhibitor AGN193109 results in increased M/L-OPSIN and reduced**
803 **S-OPSIN expression, indicating shift in cone subtype specification towards fovea-like composition.** Dosing with
804 RA receptor inhibitor AGN193109 early in differentiation (between d42-d50), mid (d70-80) and late (d120-130)
805 resulted in (a) no change in mRNA expression at d150 of (i) pan-cone marker *ARRESTIN-3* ($t(2)=0.82$, $p=0.5$;
806 $t(3)=0.43$, $p=0.88$; $t(3)=1.22$, $p=0.46$), or (ii) rod marker *RHODOPSIN* ($t(2)=1.03$, $p=0.41$; $t(3)=0.65$, $p=0.76$;

807 $t(3)=2.43$, $p=0.15$), while early+mid and early+mid+late dosing resulted in upregulation of mRNA for (iii)
808 green/red cone gene *M/L-OPSIN* approaching significance ($t(3)=1.70$, $p=0.29$/$t(3)=2.37$, $p=0.16$), and significant
809 reduction in (iv) blue cone gene *S-OPSIN* ($t(3)=1.67$, $p=0.30$; $t(3)=5.64$, $p=0.02$). Both (v) *M-OPSIN* ($t(3)=1.27$,
810 $p=0.29$/$t(3)=1.53$, $p=0.22$) and (vi) *L-OPSIN* ($t(3)=1.51$, $p=0.23$/$t(3)=2.70$, $p=0.07$) showed a trend towards
811 increasing for early+mid/early+mid+late dose, with early+mid+late for *L-OPSIN* approaching significance. (b) no
812 change in proportion of cells expressing protein (i) ARRESTIN-3 ($t(11)=1.29$, $p=0.22$); (ii) RHODOPSIN ($t(11)=0.41$,
813 $p=0.69$); or proportion of ARRESTIN-3+ cells expressing (iii) M/L-OPSIN ($t(11)=0.14$, $p=0.89$); but a significant
814 decrease in the proportion of ARRESTIN-3+ cells expressing (iv) S-OPSIN ($t(11)=3.14$, $p=0.01$). (c) Early, middle
815 and late dosing resulted in an increase in *SFRP1* expression at d150, although this only reached statistical
816 significance for triple-dosed hROs ($t(2)=2.02$, $p=0.18$; $t(3)=2.45$, $p=0.15$; $t(3)=5.04$, $p=0.02$). (c) Additionally, early
817 dosing with AGN193109 led to significant increase in *SFRP1* by d60 of differentiation ($t(4)=4.50$, $p=0.01$). All qRT-
818 PCR data shown as Log_2 fold change of CT values relative to the mean of DMSO treated controls (3-5 pooled hROs
819 per sample, n≥3, lines indicate paired samples of DMSO/AGN-dosed samples from the same batch of
820 differentiation to control for batch-batch variation.). All qRT-PCR data normalized to both *GAPDH* and *β–actin*
821 housekeeping genes. Significance values determined by paired/unpaired t-tests/one-way repeated measures
822 ANOVA followed by Dunnett's test against control group, adjusting for multiple comparisons: **p* value<0.05, ***p*
823 value<0.01, data are represented as mean ±SD. Staining data representative of n>5 hROs, counterstained with
824 DAPI (*greyscale*). Scale bars - 500μm.

825 **Supplementary Tables**

826

ALDH1A1	Rabbit	Abcam	ab23375	AB_2224009	1:200
ALDH1A3	Rabbit	Abcam	ab129815	AB_2937054	1:200
ARRESTIN-3	Goat	Novus	NBP1-37003	AB_2060085	1:100
CASPASE-3	Rabbit	Abcam	ab2302	AB_302962	1:100
CRX	Mouse	Abnova	H00001406-M02	AB_606098	1:800
KI67	Rabbit	Abcam	ab15580	AB_443209	1:100
M/L-OPSIN	Rabbit	Millipore	AB5405	AB_177456	1:100
NRL	Goat	R+D systems	AF2945	AB_2155098	1:100
ONECUT1	Mouse	Santa cruz	sc-13050	AB_2251852	1:100
OTX2	Goat	R&D Systems	AF1979	AB_2157172	1:50
RBPMS	Rabbit	PhosphoSolutions	1830	AB_2492225	1:150
RECOVERN	Rabbit	Chemicon	AB5585	AB_2253622	1:1000
RHODOPSIN	Mouse	Sigma	O4886	AB_260838	1:1000
RXRγ	Mouse	Santa Cruz	sc-365252	AB_10850062	1:200
S-OPSIN	Rabbit	Millipore	AB5407	AB_177457	1:200
SOX9	Rabbit	Sigma	AB5535	AB_2239761	1:200
VIM	Chicken	Novus	NB300	AB_922758	1:600
VSX2	Mouse	Santa Cruz	sc-365519	AB_10842442	1:200

827 **Supplementary Table 1 – Primary antibodies**

828

Gene	Forward	Reverse	Universal Probe
AIPL1	GGAGAGGGAAATCGGCTCTT	TTCTCCTTGGTCTGCAGGTT	79
ALDH1A1	GTTAGCTGATGCCGACTTGG	CGCTCAACACTCCTTCGAAC	81
ALDH1A3	AAGAGGAGATTTTCGGGCCA	ACTTCAGGGCTTTGTCGAGA	66
ARR3	CACGGAGACTGTAGCTGCTA	GCTAGAGGCCAGGTTGGTAT	14
β-ACTIN	GCACCCAGCACAATGAAGAT	TCGTCATACTCCTGCTTGCT	63
CRX	GAGGCTGTGTCTTGTGCAAA	TCGAAGTCTTACCCCATCGG	12
CRABP2	CCCTGTAAGAGCCTGGTGAA	CCGTCATGGTCAGGATCAGT	93
CYP16A1	GACATGCAGGCACTAAAGCA	GGTAGAGCCCCAGGTAAGTG	5
FGF8	GAGACGGGCCTCTACATCTG	TGTACCAGCCCTCGTACTTG	67
FGFR1	CGGGACAGACTGGTCTTAGG	GGTTGGGTTTGTCCTTGTCC	53
FGFR2	CAGTCATCCTGTGCCGAATG	AACTGTTACCTGTCTCCGCA	71
FGFR3	TACTCCTTCGACACCTGCAA	ACTTCTGGGAGGCCAAGTAC	68
FGFR4	GGAGTCCCGGAAGTGTATCC	GTAGTCAATGTGGTGGACGC	71
GAPDH	TTGCCCTCAACGACCACTTT	TGGTCCAGGGGTCTTACTCC	77
ISLET1	TCTCCGGATTTGGAATGGCA	CATTTGATCCCGTACAACCTGAT	-
L-OPSIN	TGCATCATCCCACTCGCTAT	TTCCTTCTCTGCCTTCTGGG	5
M-OPSIN	CTACCTCCAAGTGTGGCTGG	GAATGCCAGGACCATCACCA	13
M/L-OPSIN	CTTCCACCCTTTGATGGCTG	AGTTTCGAAACTGCCGGTTC	-
NRL	AGAGCTGTGTGCAGAAGTCT	GCAGAAGTCGTCCAATCCAC	95
ONECUT1	CAGCGTCGAACTCTACATGC	ACTCCTCCTTCTTGCGTTCA	3
OTX2	ATTGCTAGAGCAGCCCTCAC	GGAGCAGTGGAACTTACAGC	-
RBPMS	CACTGCATGCCCAGATGC	CCCACAAGACAGATTGCAGC	-
RCVRN	GCTTCGATTCCAACCTCGAC	TTACCGTCCACGTCGTAGAG	78
RHODOPSIN	TGGGCCATTAAAAGCTCAGC	GTGGAAGCTGGCAGTTTCAA	77
RXRγ	CATGAAGAGGGAAGCTGTGC	TTCTGCCTCACTCTCAGCTC	82
SFRP1	GCCCGAGATGCTTAAGTGTG	GACACACCGTTGTGCCTTG	-
S-OPSIN	GCACTGTAGCAGGTCTGGTT	CAATGGTCCAGGTAGCCAGG	72
THRβ	ATTTCGTTCTCCGGTCCTGT	TCAAGTCTTGGACCAGGGAC	9
VSX2	TGGGGATGCACAAAAAGTCG	GCTCCATCTTGTCGAGCTTG	69

Supplementary Table 2 – Primers

Supplementary Figures

Supplementary Figure 1. Serial sections of a single human fetal retina (CS20) show expression of *CYP26A1* is localized to a single spot-like region at the presumptive macula (PM), while *FGF8* is exclusively expressed around the optic nerve head. (a) Representative images of serial sections through a CS20 human retina, taken at 100µm intervals and stained for the RA catabolizing enzyme, *CYP26A1* (*magenta*), and growth factor *FGF8* (*cyan*) mRNA using RNAscope™. Imaging shows expression of *CYP26A1* in the PM with no overlapping *FGF8* expression, which is instead expressed around the optic nerve head. White arrows indicate PM, while white outlined arrow heads indicate low levels of *CYP26A1* expression visible around optic nerve head (ONH) and at nasal edge of the retina. Sections were co-stained with RPC marker, VSX2 (*green*) and counterstained with nuclear marker, DAPI (*greyscale*). S – Superior; I – Inferior; PCW – Post-conception Weeks. Images taken at 20x magnification. Images are representative of n=3 CS20/21 samples. Scale bars - 500µm.

Supplementary Figure 2. Proliferation in human developing retinal regions (CS18-23)
(a), Masking of macular (based on *CYP26A1*+ staining), central (adjacent to the optic nerve), nasal (equivalent distance as macula to periphery on the central-peripheral gradient on the nasal side) and peripheral regions in Imaris 10.0. (b) Proportion of KI67+ cells in all analyzed developing retinal regions from CS18-23, showing the macula has a similar proportion of KI67+ cells to the peripheral retina at CS18 (mean of 65/66% respectively, t(2)=0.33, *p*=0.78)), and significantly different to central/nasal regions (t(2)=2.24, *p*=0.16; t(2)=2.05, *p*=0.18), while at CS20/23, the macula had similar proportion of KI67+ cells to the central retina (CS20: means of 34/36%, t(2)=1.15, *p*=0.37); CS23: means of 24/22%, t(2)=0.38, *p*=0.74) and significant/nearing significant difference in proliferating cells compared with nasal/peripheral retina (CS20: t(2)=5.26, *p*=0.03/t(2)=5.92, *p*=0.02; CS23: t(2)=2.47, *p*=0.13/t(2)=2.76, *p*=0.11 respectively. (c) Linear regression of proportion of KI67+ cells in different retinal regions between CS18 and CS20 shows that the macular region has a steeper decline in KI67+ cells than any other retinal region (macula: -15.62, central: -5.5, nasal: -8.7, peripheral: 0.8, *p*=0.01). n=3/timepoint, data are represented as mean ±SD.

Supplementary Figure 3. Temporal and spatial photoreceptor development in human retinal organoids.
(a) graphical representation of hRO differentiation and "early" dosing with RA receptor inhibitor AGN193019 (10µM) and recombinant FGF8 (100ng/ml) between d42-50, followed by "mid" AGN193109 pulse at d70-80 and "late" pulse at d120-130; (b-d) Relative mRNA expression of (b) RPC cell marker *VSX2* showing upregulation at d40 of differentiation compared with d0, (c) photoreceptor precursor markers, *RECOVERIN*, *CRX* and *AIPL1* showing photoreceptor specification from d40 of differentiation with expression further increasing to d90 and (d) cone precursor markers *RXRγ*, *THRβ* and *ONECUT1* significantly upregulated by d40, with plateauing expression from d60-70, indicating specification of cone precursors by this timepoint; (e) immunostaining of VSX2+ retinal progenitor cells in the neuroblastic layer (NBL) from d40 of differentiation, along with retinal ganglion cell (RGC) marker RBPMS in the inner nuclear layer (INL) from d60, OTX2+ cone-biased progenitor cells showing increasing cell numbers from d50, and RECOVERIN+ photoreceptor precursors from d70 predominantly localizing to the outer layers of developing hROs, and ONECUT1+ horizontal cell-biased retinal progenitors towards the inner layers of the organoid, alongside some OTX2+/RECOVERIN+ bipolar cells/mis-localized photoreceptor precursor cells; (f) Relative mRNA expression of mature cone markers *ARR3, OPSNSW, OPSNMW* and *OPSNLW* and (g) mature rod markers *RHODOPSIN*, *NRL* and photoreceptor marker *RECOVERIN* showing maturation of rods and cones by d150 of differentiation; (h) immunostaining of mature d150 retinal hROs stained for pan-photoreceptor marker RECOVERIN, with tight multilayered NRL+ rod nuclei in the outer nuclear layer (ONL), RHODOPSIN labelling the outer segments of rod photoreceptor cells and ARR3 labelling the cell bodies of a single apical layer of cone photoreceptor cells showing the inner segments, with a small number of S-OPSIN+ short wavelength cones, and M/L-OPSIN+ medium/long wavelength cones, with some RECOVERIN+ photoreceptors displaced to the INL. All qRT-PCR data shown as Log_2 fold change of CT values relative to d0 hESCs (3-5 pooled hROs per sample, n=3). qRT-PCR data normalized to both *GAPDH* and *β-actin* housekeeping genes. Significance values determined by one-way repeated measures ANOVA followed by Dunnett's test against control

group, adjusting for multiple comparisons: *p value<0.05, **p value<0.01, ****p value<0.0001, data are represented as mean ±SD. Staining data representative of n=3 hROs, counterstained with DAPI (*greyscale*). Scale bars - 100μm.

Supplementary Figure 4 – Dose optimization of AGN193109 and recombinant FGF8 for hROs based on alamarBlue cell viability assay. Fluorescence was measured at 590nm (RFU) and change in reduction at d4 and d8, compared with d0 of dosing for each hRO, then relative change of treated compared with DMSO treated was calculated and plotted for (a) AGN193109 and (b) recombinant FGF8 (rFGF8) (n=5). (c) Dosing with rFGF8between d40-d50 lead to no significant change in *FGF8,* which is known to regulate its own expression Data shown as Log_2 fold change of CT values relative to PBS treated controls (5 pooled hROs per sample, n=4). Data normalized to both *GAPDH* and *β–actin* housekeeping genes. Error bars - standard deviation. Significance values determined by one-way repeated measures ANOVA followed by Dunnett's test against control group, adjusting for multiple comparisons. *p value<0.05.

Supplementary Figure 5. Dosing early hROs with RA receptor inhibitor AGN193109 does not alter retinal ganglion cell (RGC) marker or cone precursor marker expression at d60. (a-b) Dosing with RA receptor inhibitor AGN193109 between d40-d50 leads to (a) a significant reduction in *CRABP2,* a proxy for circulating RA levels, (t(2)=5.77, p=0.03), (b) but no significant change in RGC marker *RBPMS* (t(4)=1.02, p=0.37) or RGC/bipolar/amacrine cell marker *ISLET1* (t(4)=0.30, p=0.78). Lines indicate paired samples of DMSO/AGN-dosed samples from the same batch of differentiation to control for batch-batch variation. All data shown as Log_2 fold change of CT values relative to the mean of DMSO treated controls (5 pooled hROs per sample, n≥3, lines indicate paired samples of DMSO/AGN-dosed samples from the same batch of differentiation to control for batch-batch variation). All qRT-PCR data normalized to both *GAPDH* and *β–actin* housekeeping genes. Significance values determined by paired t-tests. (c) Immunostaining of AGN193109 dosed and DMSO dosed control hROs at d60 showing no significant change in the proportion of (i) RGC marker RBPMS *(yellow)* cells (t(30)=0.08, p=0.94) (ii) cone precursor marker RXRg (*red*) (t(26)=0.96, p=0.35) or (iii) RPC marker VSX2 (staining in Figure 6) (t(29)=0.01, p=0.99). Significance values determined by unpaired t-tests: *p value<0.05, n>13, data are represented as mean ±SD. Staining data representative of n>13 hROs, counterstained with DAPI (*greyscale*). Scale bars - 100μm.

Supplementary Figure 6 – Masking of necrotic core for CASPASE-3 staining quantification in IMARIS 10.0.

a

PCW6 CS16/17 | PCW7 CS18/19 | PCW8 CS20/21 | PCW8 CS22/23

FGF8/CYP26A1/VSX2/DAPI

FGF8/CYP26A1

PCW10 | PCW12 | PCW16/17

FGF8/CYP26A1/VSX2/DAPI

FGF8/CYP26A1

b

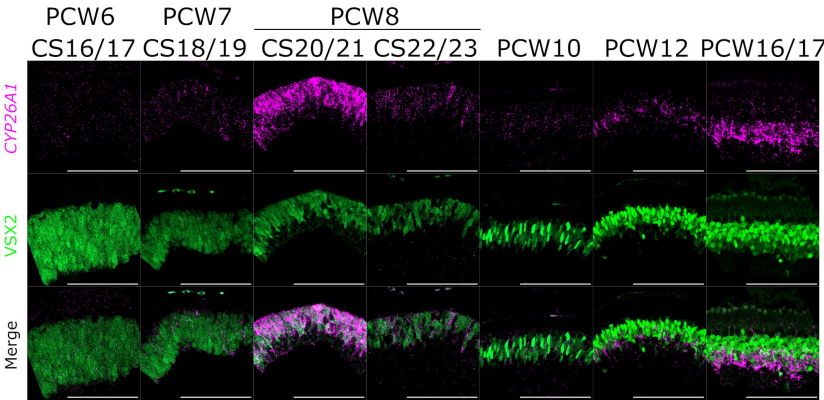

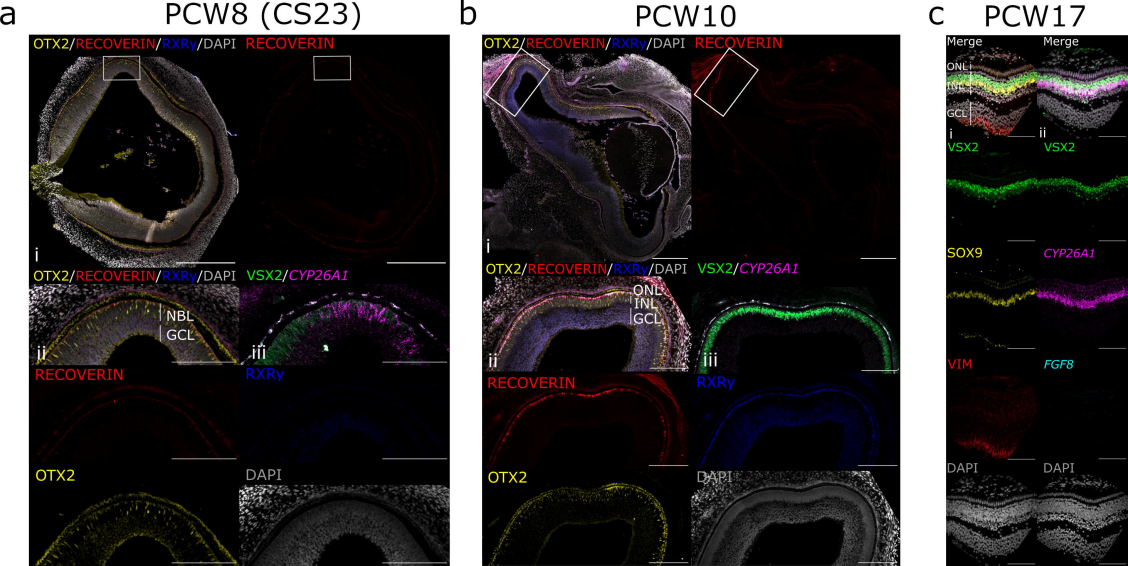
a
PCW8 (CS23)
OTX2/RECOVERIN/RXRγ/DAPI
RECOVERIN
i
OTX2/RECOVERIN/RXRγ/DAPI
VSX2/CYP26A1
NBL
GCL
ii
iii
RECOVERIN
RXRγ
OTX2
DAPI
b
PCW10
OTX2/RECOVERIN/RXRγ/DAPI
RECOVERIN
i
OTX2/RECOVERIN/RXRγ/DAPI
VSX2/CYP26A1
ONL
INL
GCL
ii
iii
RECOVERIN
RXRγ
OTX2
DAPI
c
PCW17
Merge
Merge
ONL
INL
GCL
i
ii
VSX2
VSX2
SOX9
CYP26A1
VIM
FGF8
DAPI
DAPI

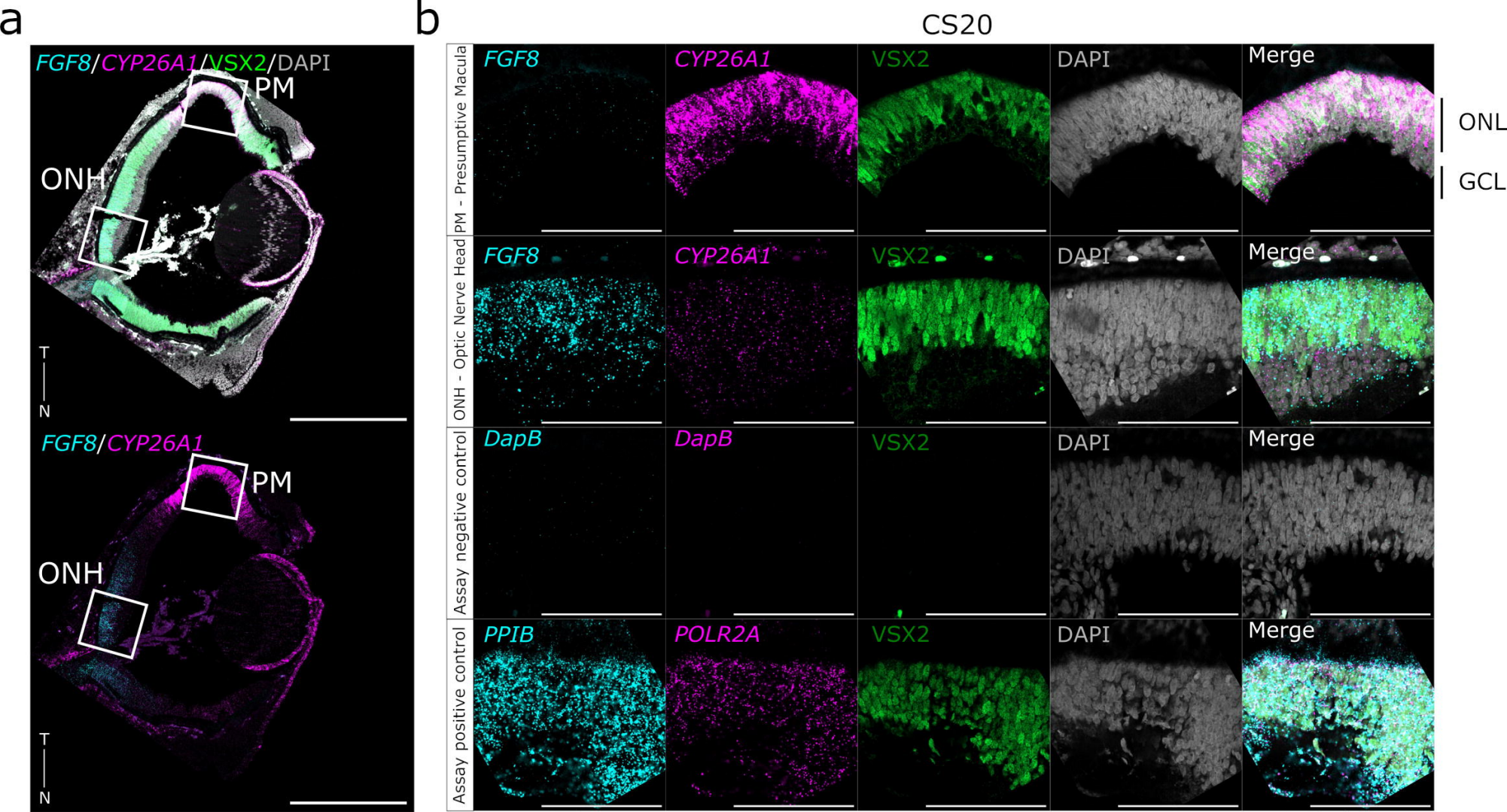
a
FGF8/CYP26A1/VSX2/DAPI
PM
ONH
T
N
FGF8/CYP26A1
PM
ONH
T
N
b
CS20
PM - Presumptive Macula
ONH - Optic Nerve Head
Assay negative control
Assay positive control
FGF8
CYP26A1
VSX2
DAPI
Merge
FGF8
CYP26A1
VSX2
DAPI
Merge
DapB
DapB
VSX2
DAPI
Merge
PPIB
POLR2A
VSX2
DAPI
Merge
ONL
GCL

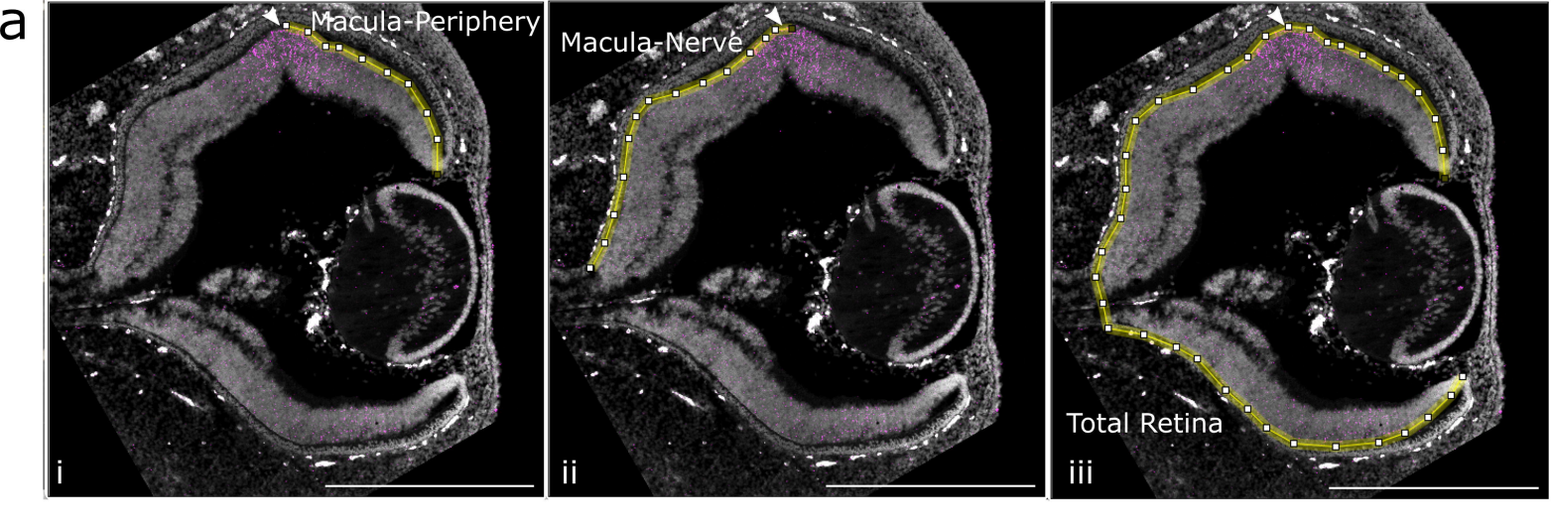
a
Macula-Periphery
Macula-Nerve
Total Retina
i
ii
iii

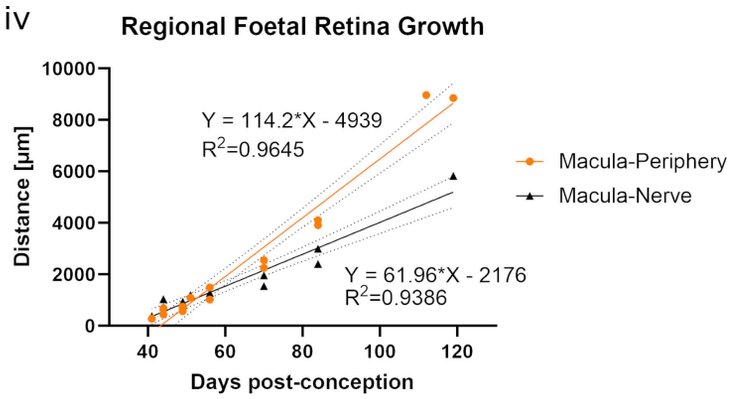
iv
Regional Foetal Retina Growth
Distance [µm]
Days post-conception
Y = 114.2*X - 4939
R2=0.9645
Y = 61.96*X - 2176
R2=0.9386
Macula-Periphery
Macula-Nerve

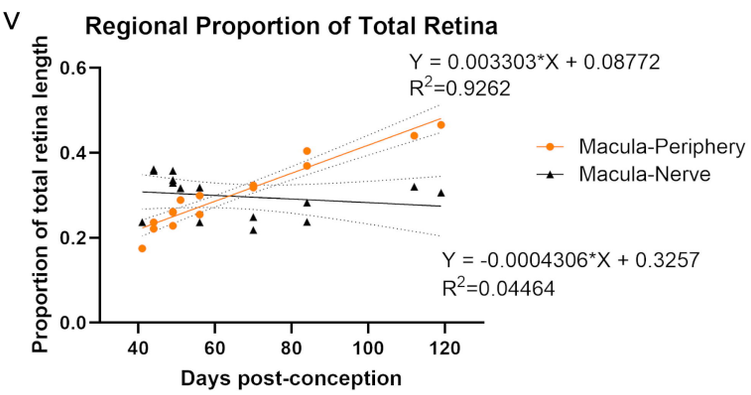
v
Regional Proportion of Total Retina
Proportion of total retina length
Days post-conception
Y = 0.003303*X + 0.08772
R2=0.9262
Y = -0.0004306*X + 0.3257
R2=0.04464
Macula-Periphery
Macula-Nerve

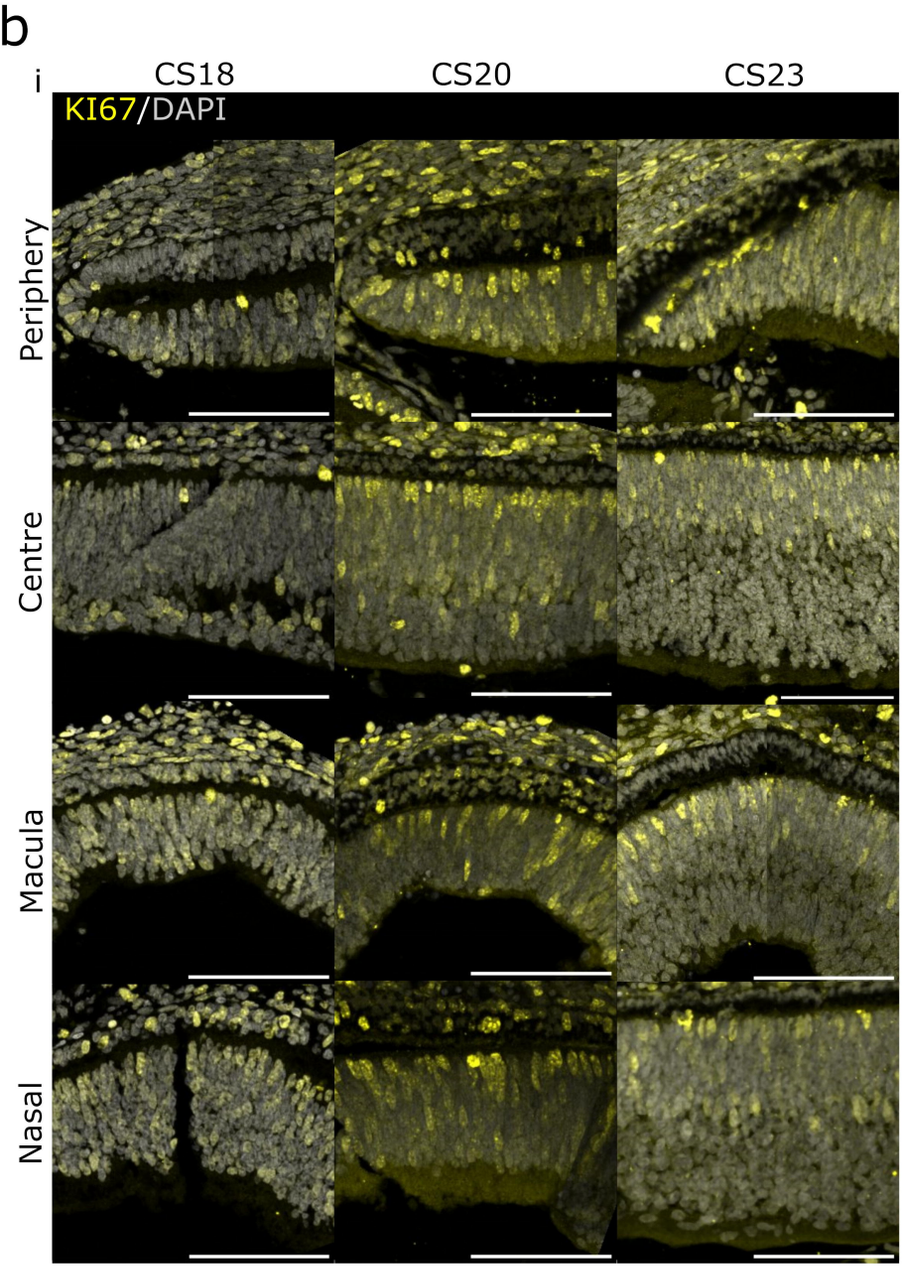
b
i
CS18
CS20
CS23
KI67/DAPI
Periphery
Centre
Macula
Nasal

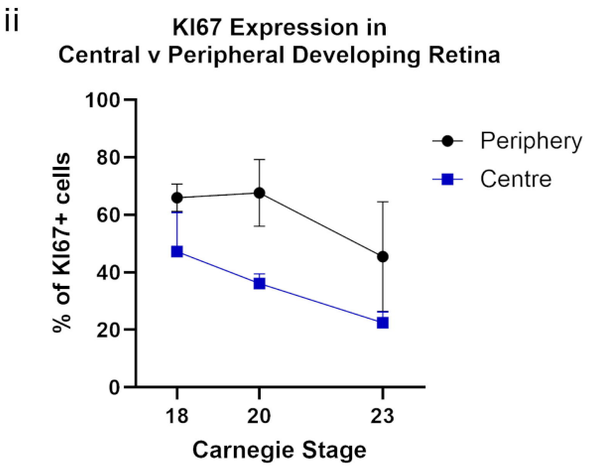
ii
KI67 Expression in
Central v Peripheral Developing Retina
% of KI67+ cells
Carnegie Stage
Periphery
Centre

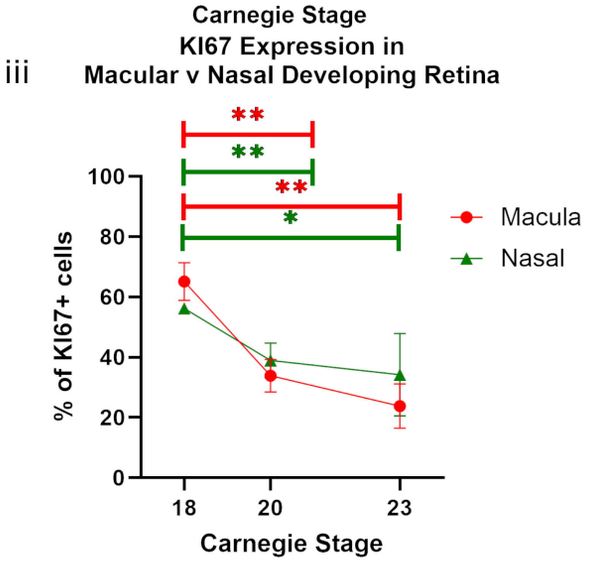
iii
KI67 Expression in
Macular v Nasal Developing Retina
% of KI67+ cells
Carnegie Stage
Macula
Nasal

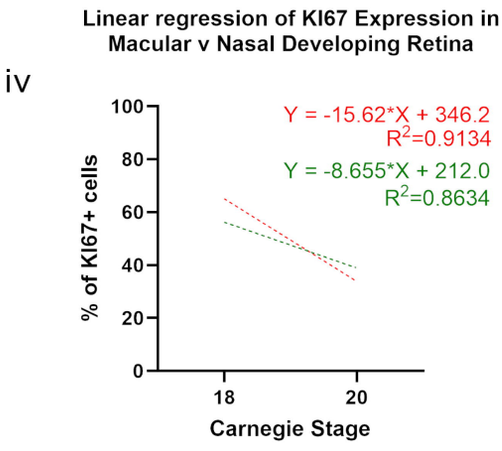
Linear regression of KI67 Expression in
Macular v Nasal Developing Retina
iv
% of KI67+ cells
Carnegie Stage
Y = -15.62*X + 346.2
R2=0.9134
Y = -8.655*X + 212.0
R2=0.8634

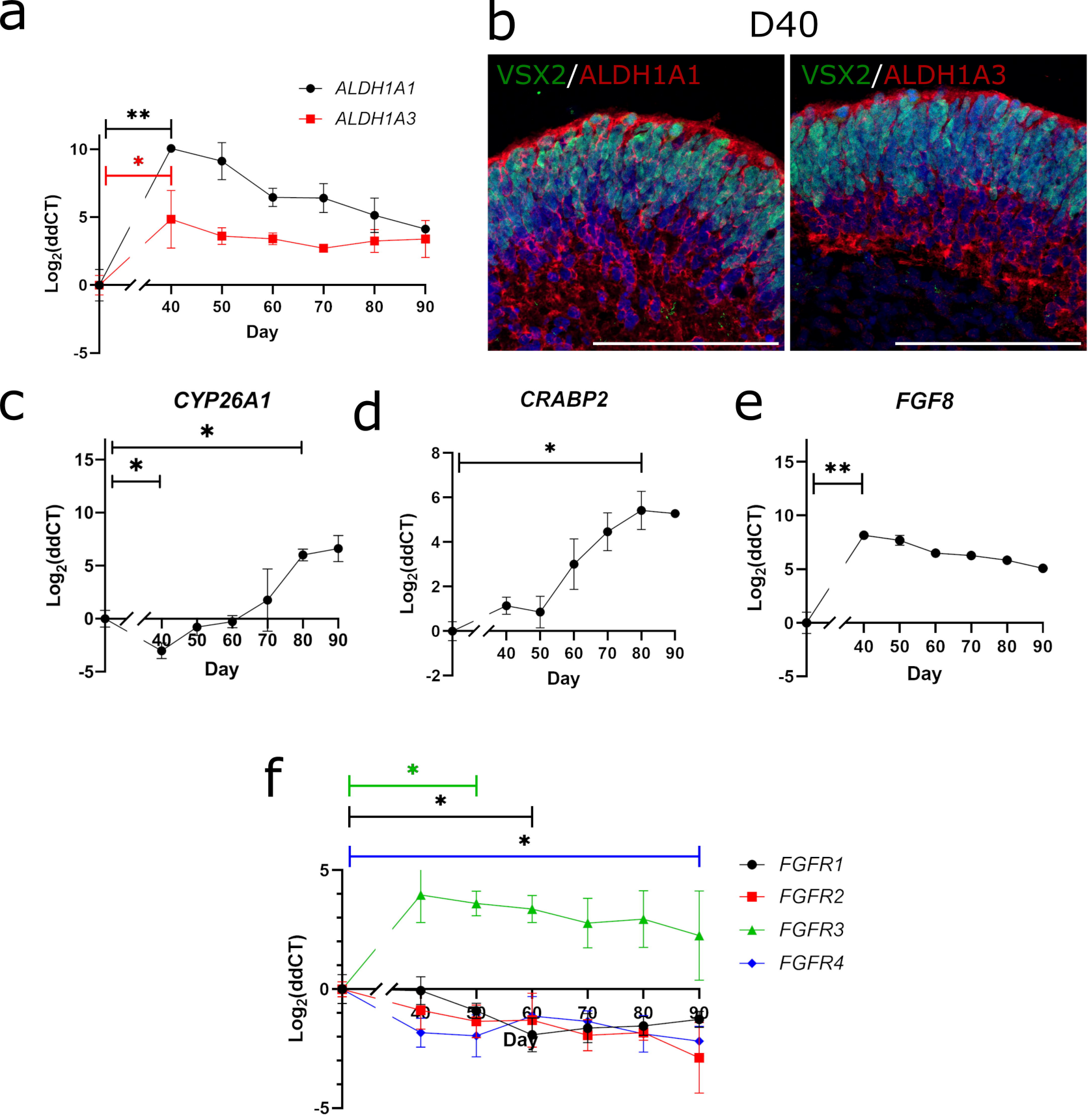
a
ALDH1A1
ALDH1A3
**
*
Log2(ddCT)
Day
b
D40
VSX2/ALDH1A1
VSX2/ALDH1A3
c
CYP26A1
d
CRABP2
e
FGF8
f
FGFR1
FGFR2
FGFR3
FGFR4

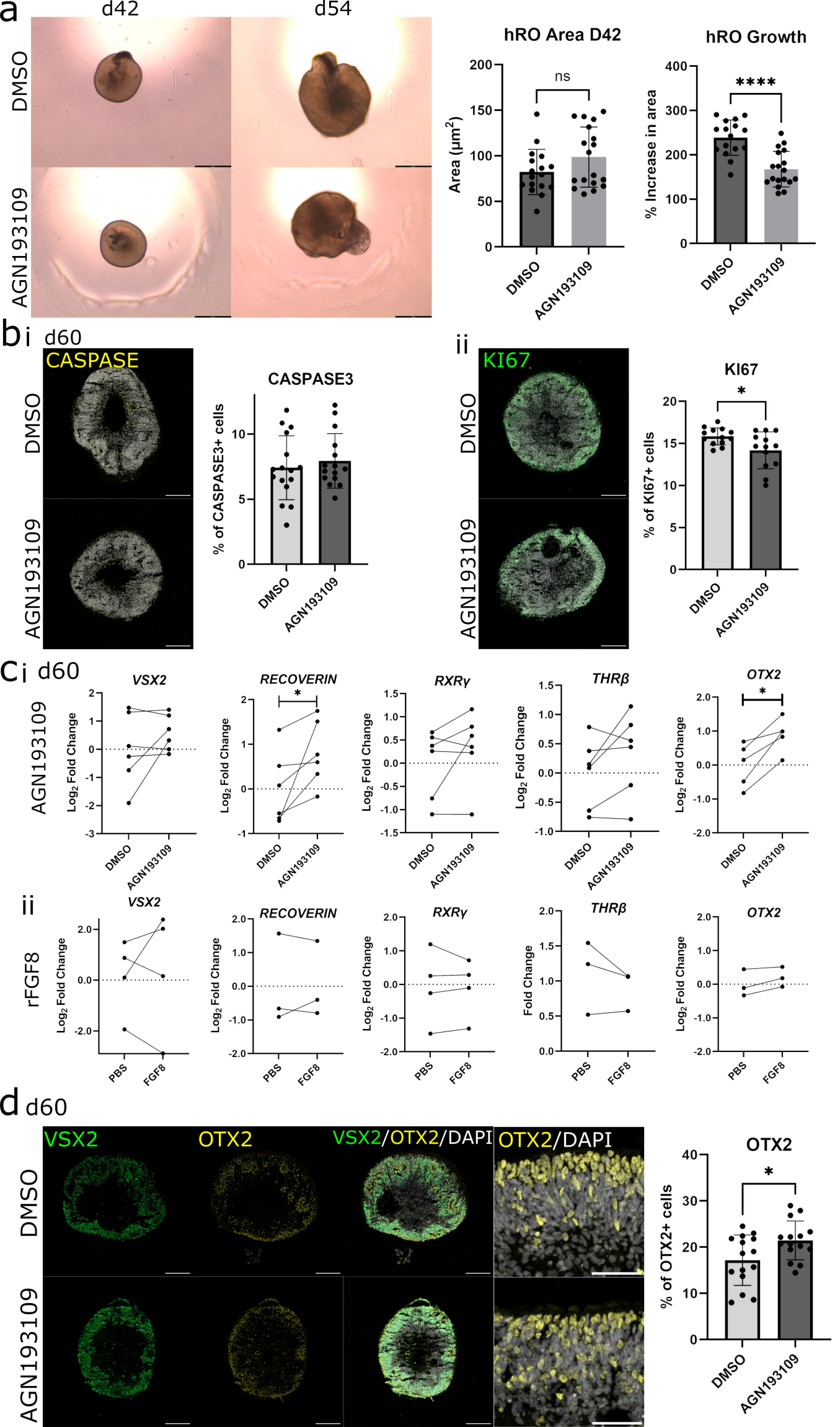
a
d42
d54
DMSO
AGN193109
hRO Area D42
ns
Area (µm²)
hRO Growth
****
% Increase in area
b i d60
CASPASE
CASPASE3
% of CASPASE3+ cells
ii
KI67
% of KI67+ cells
*
c i d60
VSX2
RECOVERIN
RXRγ
THRβ
OTX2
Log₂ Fold Change
Fold Change
PBS
FGF8
rFGF8
d d60
VSX2/OTX2/DAPI
OTX2/DAPI
% of OTX2+ cells

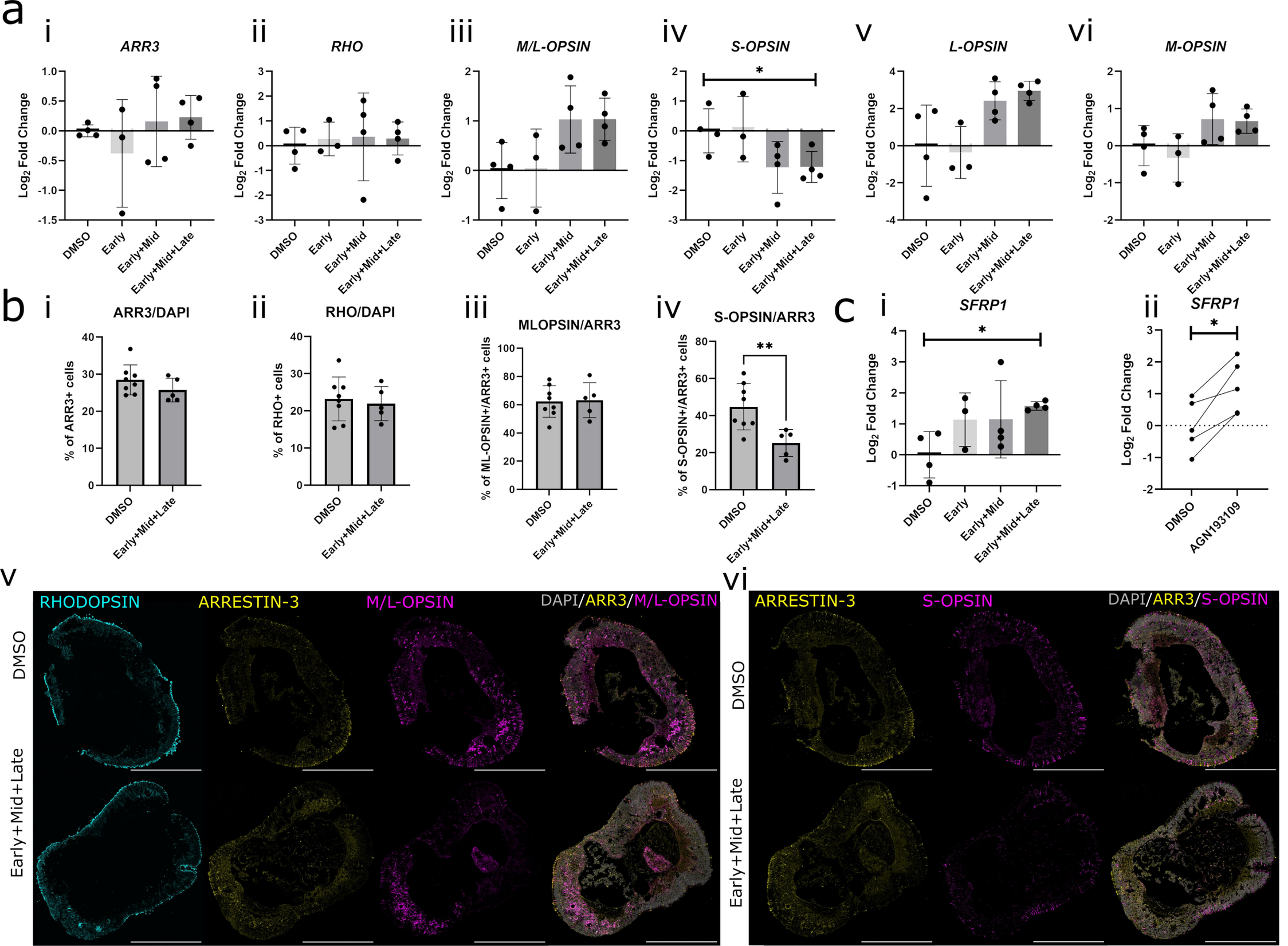
a
i
ARR3
ii
RHO
iii
M/L-OPSIN
iv
S-OPSIN
v
L-OPSIN
vi
M-OPSIN
Log2 Fold Change
DMSO
Early
Early+Mid
Early+Mid+Late
b
i
ARR3/DAPI
% of ARR3+ cells
ii
RHO/DAPI
% of RHO+ cells
iii
MLOPSIN/ARR3
% of ML-OPSIN+/ARR3+ cells
iv
S-OPSIN/ARR3
% of S-OPSIN+/ARR3+ cells
c
i
SFRP1
ii
SFRP1
AGN193109
v
RHODOPSIN
ARRESTIN-3
M/L-OPSIN
DAPI/ARR3/M/L-OPSIN
vi
ARRESTIN-3
S-OPSIN
DAPI/ARR3/S-OPSIN